RETROFIT55

Ref. Ares(2025)3459014 - 29/04/2025

Funded by the European Union

Horizon Europe programme, grant agreement No. 101096068S

RETROFIT SOLUTIONS TO ACHIEVE 55% GHG REDUCTION BY 2030

Report on the performance prediction based on advanced dynamical system

WP 2 – Hydrodynamic design optimization
Task 2.4 – Dynamical system for performance prediction
D2.4 – Report on the performance prediction based on advanced dynamical system
Partners involved: NTUA, AALTO, SFD, FSYS, CNR, RINA, LASK, AES, ATD
Authors: K.Belibassakis, N.Themelis, G.Dafermos

Project details

Project Title	RETROFIT SOLUTIONS TO ACHIEVE 55% GHG REDUCTION BY 2030
Project Type	Innovation Action
Project Acronym	RETROFIT55
Grant Agreement No.	101096068
Duration	36 M
Project Start Date	01/01/2023

Deliverable information

Status (F: final; D: draft; RD: revised draft)	F
Planned delivery date	31/03/2025
Actual delivery date	29/04/2025
• **Dissemination level:** PU – Public, fully open, e.g. web (Deliverables flagged as public will be automatically published in CORDIS project's page) • SEN – Sensitive, limited under the conditions of the Grant Agreement • Classified R-UE/EU-R – EU RESTRICTED under the Commission Decision No2015/444 • Classified C-UE/EU-C – EU CONFIDENTIAL under the Commission Decision No2015/444 • Classified S-UE/EU-S – EU SECRET under the Commission Decision No2015/444	PU
Type: Report, Website, Other, Ethics	Report

Document history

Version	Date	Created/Amended by	Changes
1	17.01.2025	K.Belibassakis & N.Themelis	
2	12.03.2025	K.Belibassakis, N.Themelis, G.Dafermos (NTUA)	Addition of Sub-Section 4.4 and Appendix C.
3	14.04.2025	K.Belibassakis, N.Themelis, G.Dafermos (NTUA)	Version after technical review
4	27.04.2025	K.Belibassakis, N.Themelis, G.Dafermos (NTUA)	Version after editorial review

Quality check review

Reviewer (s)	Main changes / Actions
Hannes Renzsch (FYST)	Technical revision.
Emanuele Spinosa and (CNR)Cecilia Leotardi (CNR)	Editorial revision.
Cecilia Leotardi & Alessandro Iafrati (CNR)	Final review of contents and submission to EC.

Table of contents

List of figures

List of tables

List of abbreviations

BC ship	Bulk Carrier
BEM	Boundary Element Method
DOF	Degree of Freedom
DSS	Decision Support System
DWT	DeadWeight
GHG	Greenhouse Gas Emissions
ITTC	International Towing Tank Conference
MCR	(Ship Engine) Maximum Continuous Rating
RPM	Revolutions Per Minute
SHP	Main Engine Shaft Horse Power
VLM	Vortex Element Model

Executive Summary

Ship propulsion performance in moderate and more severe sea-states is significantly affected due to ship motions and added wave resistance, as well as wind resistance and other factors. All the above cause additional energy losses that could reduce the propulsion system performance, resulting in involuntary speed reduction and excessive fuel consumption.

In particular, the effects of wave-induced vertical stern ship motion on the propulsive thrust and efficiency, which are examined by an unsteady Vortex Element Model for the propeller operating in the wake field of the ship, can provide useful information and related data that can be exploited for the definition of the parameters of a dynamical system for the prediction of ship performance in waves. Results from the propeller hydrodynamic analysis, in conjunction with seakeeping analysis in regular and irregular waves, are subsequently used to obtain ship propulsion performance predictions by means of the above dynamical model.

In the case of the Bulk Carrier examined in the framework of RETROFIT55 project, systematic predictions of the ship responses and added wave resistance calculated for a variety of loading conditions, including full load, normal and heavy ballast and laden conditions (with trim), are used to illustrate the applicability of the dynamical model for the prediction of ship performance in different sea states and various wave directions. The obtained results could be further exploited to study the benefits of ship speed and engine RPM control from the point of view of optimizing ship's propulsive performance and reducing energy losses.

The structure of the present report is as follows: after a short introduction concerning the simulation methods for unsteady propeller performance, including also information about the selection of ship and equipment data, which is used for demonstration, the dynamical model for the ship propulsion performance in waves is presented in Section 2. Subsequently, a method for the unsteady analysis of marine propellers based on Vortex Element Model is discussed, which is used, in conjunction with seakeeping analysis to estimate various quantities and define the coefficients involved in the dynamical model. Next the application to the case of the bulk carrier MV Kastor is discussed and results related to the performance of the ship and propeller, as well as data covering the responses and mean added wave resistance obtained from standard seakeeping analysis, are presented. The latter information and data are subsequently used to demonstrate the performance prediction of the ship in waves based on the elaborated dynamical system. Discussion and conclusions are provided in the last section of the present report. Finally, in Appendix A the data referring to the studied bulk carrier for various selected loading conditions, in Appendix B results from seakeeping analysis including data regarding the calculated mean wave added resistance for various conditions (ship loading and speed, wave conditions and direction etc) and in Appendix C a parametric analysis on the effect of the wave velocities and seakeeping response on the operational performance, are provided.

The present analysis will support the development of surrogate models in WP1 and WP3 which will be used for the ship performance prediction in various sea states and wind/wave directions.

1 Introduction

Requirements and inter-governmental regulations for greening waterborne transport have become more stringent in defined steps, especially concerning the development and demonstration of decarbonisation solutions and technologies in shipping, which can be used by ship owners to reduce Greenhouse Gas (GHG) emissions and fuel consumption by at least 55% before 2030 compared to 2008. In particular, propulsion technology for reduced pollution and environmental impact and response to the demand has been recognized to be an important factor regarding global warming and climatic change. Thus, environmentally friendly technical solutions with reduction of exhaust gases are required. Additionally, the increased competition in the field of maritime technology requires even more economical vessels. Therefore, optimization of ship propulsion performance in realistic conditions has become a central issue.

Well known technologies addressed to reduce the GHG emissions cover, except for the hydrodynamic design optimization related to minimization of hull resistance and optimization of propulsion efficiency [1], the exploitation of Energy Saving Devices and renewable energy, from wind, waves and solar energy, ship electrification and improved management of the operational phase and the on-board systems. The calculation cost of the wave resistance of a ship can be reduced by model testing and systematic application of modern design Computational Fluid Dynamics tools. The frictional resistance of a ship may be reduced by injection of micro bubbles, using air films and polymers, super water repellent coatings, magneto-hydrodynamics and surface shaping; details can be found in ITTC [2]. Among several methods Air Lubrication Systems and Wind Assisted Propulsion are examined today for providing combined with design optimization an achievable solution (see, e.g., [3]). In the case of WASP-equipped ships [4] induced heel and drift angles are expected to further affect the propeller behaviour.

Moreover, external factors such as waves and other components influence the actual flow on the propeller and affect the behaviour of the propulsion system. However, the ships rarely operate in calm sea, and in realistic sea states and adverse conditions additional components come into play, as e.g. added wave and wind resistance, as well as the effect of ship's stern motion on the propeller-hull interaction. Moreover, propellers and ship hulls get fouled. Several studies (see e.g., [5]) report achievable gains of ship energy losses of the order of 5% by exploiting accurate monitoring to better control the propulsion train.

In previous tasks of RETROFIT55 project the effects of wave-induced motions of the ship on the modification of propulsive thrust and efficiency are examined by means of Unsteady Vortex Element Method (VLM) used for the analysis of moving propeller(s) in the wake field of the ship; see also [6]. Information associated with the oscillatory vertical stern and propeller motion in waves can be provided by seakeeping analysis of the hull in regular and irregular waves.

Results from the propeller unsteady analysis, in conjunction with seakeeping analysis in regular and irregular waves, are used for the definition of the parameters of a simplified system developed for the prediction of ship performance in waves. Results from the present hydrodynamic analysis, in conjunction with predictions of added resistance, are used to illustrate applicability in the case of an 82000DWT Bulk Carrier, investigating the benefits of ship speed and engine RPM control from the point of view of optimizing ship's propulsive performance and reduction of energy losses. The present analysis could further support the development of non-linear, multi-DOF dynamical systems that will be used for the ship performance prediction in various sea states and wind/wave directions, as well as for the optimal design of the considered systems.

1.1 Ship and equipment data

Bearing in mind the wider needs of the project, a size criterion was applied to select a ship type out of the available vessels of LASKARIDIS Shipping, for which the examination of retrofit measures was considered practicable and meaningful. In the present work, the case of the Bulk Carrier MV Kastor of DWT82000 will be examined. This ship has already been used as a test case in previous Tasks of the project (see [7]). Table 1 presents the main characteristics of the ship, and more details are provided in Appendix A.

Table 1: Main characteristics of the ship under examination: MV Kastor

Length overall [m]	229.00
Length between perpendiculars [m]	225.50
Breadth, moulded [m]	32.26
Depth, moulded [m]	20.05
Summer load line draught, moulded [m]	14.45
Deadweight at summer load draught [t]	80996.1

1.2 Operational data for the identification of loading conditions

Figure 1 presents the routes of the MV Kastor during the monitoring period, starting from February 2021 to June 2023. Available data sources include a dataset generated by a high-frequency automatic logging system, a noon report dataset for the same period as well as weather data from a third-party provider. In D3.1 [7], a dataset was compiled from the available data sources to be utilised for the ship operational analysis. Based on this analysis, the identification of loading conditions was performed.

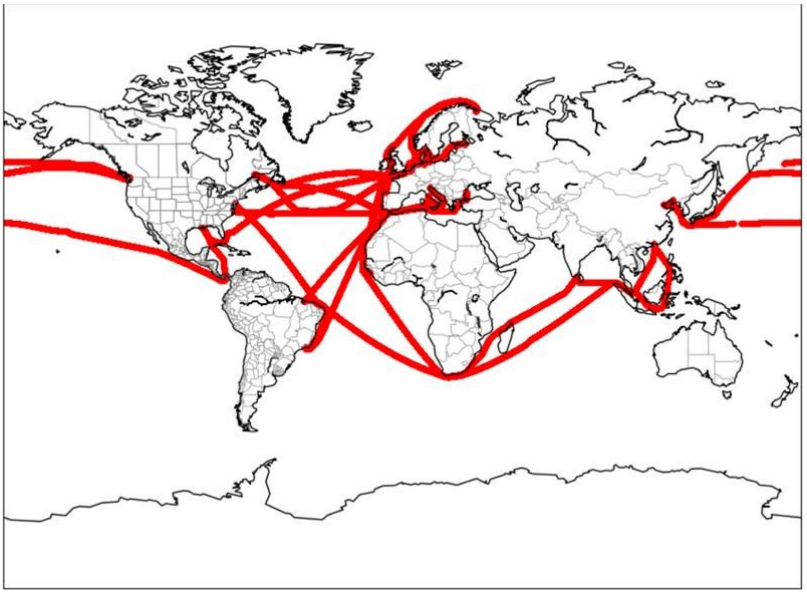

Figure 1: BC ship path on the world map during the recording period, utilizing high-frequency GPS signals.

The analysis of operational data, acquired during the reporting period, led to the identification of a certain set of loading conditions. Each loading condition is characterized by a specific mean draft. To exclude port calls, only data points with speed through water (STW) values over 6 knots are considered. In Figure 2 the distribution of the mean draft is shown, which appears to be multimodal; the four peaks protruding near the values of 6.3 m, 8.1 m, 13.2 m and 14.3 m correspond to four

discrete loading conditions: two laden and two ballast. The draft range of each loading condition, as listed in Table 2, is determined by the spread of the distribution around these peaks. Additionally, the trim is calculated by subtracting the aft from the fore draft measurement. The ship's speed range corresponding to each loading condition is shown in

Table 3. Following the data analysis discussed and the definition of the set of operational loading conditions, this task utilizes the stability booklet of MV Kastor to select the closest reported loading conditions that represent the operational profile of the ship. The identified loading conditions and the range of ship's speed for each one of them are listed in more detail in Appendix A, Table 14.

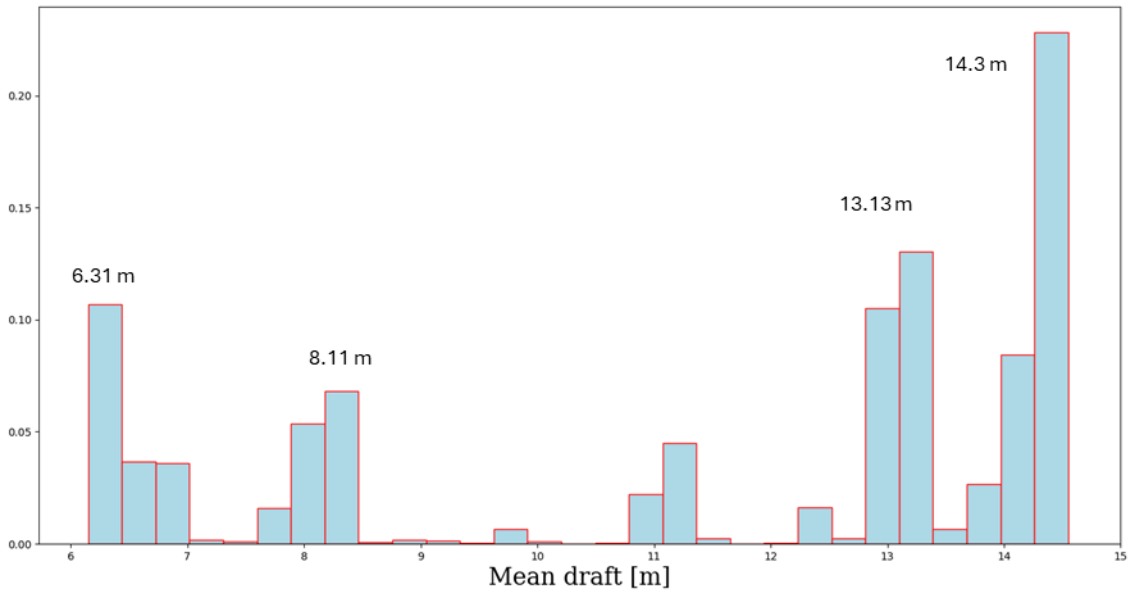

Figure 2: Histogram of the mean draft and corresponding loading conditions.

Table 2: Definition of loading conditions using Mean Draft ranges

Loading condition	Type	Draft range [m]
1	Laden	TM > 13.5
2	Laden	12 < TM < 13.5
3	Ballast	6 < TM < 6.5
4	Heavy ballast	7.75 < TM < 8.5

Table 3: Mean value and range for mean draft, trim and STW per loading condition

Loading condition	TM [m] Mean	TM [m] Range	Trim [m] Mean	Trim [m] Range	STW [kn] Mean	STW [kn] Range
1	14.30	[13.5, 14.5]	-0.16	[-0.5, 0]	12.24	[9, 15]
2	13.13	[12, 13.5]	-0.16	[-0.5, 0]	12.45	[11, 15]
3	6.31	[6, 7]	-2.89	[-3.5, -1.8]	12.94	[9, 16]
4	8.11	[7.75, 8.5]	-2.01	[-3, -1.5]	12.52	[9, 16]

2 Dynamical model for ship propulsion performance in waves

A possible approach for the prediction of the propulsive behaviour of the ship and propeller in waves (see, e.g., [8]) is based on the application of the surge equation of the ship in waves with excitation by the waves and the propeller thrust, as follows:

$$(1-t)N_p T_p + T_{WASP} - (R + R_{AW}) + F_1 = (m + a_{11})\ddot{\varsigma}_1 + b_{11}\dot{\varsigma}_1 \qquad \text{Eq. 1}$$

where $\dot{\varsigma}_1$ is the surge velocity, N_p is the number of propellers and T_p denotes each propeller's thrust, $1-t$ is the thrust deduction. Additional thrust components, such as thrust from wind assisted propulsion systems, are denoted by T_{WASP}. Also, the ship resistance (possibly including effects from Air Lubrication System) at given ship speed V_S is denoted by R, and the mean added wave resistance by R_{AW}. The latter is dependent essentially on the ship response in waves, more significantly on oscillations in the heave and pitch mode, and is usually estimated by means of standard seakeeping analysis. In the right-hand side of the above equation m is the ship mass, a_{11}, b_{11} are the added mass and hydrodynamic damping coefficients in surge motion, and F_1 the wave excitation surge force, respectively. The above model is consistent with an excitation in regular waves; however, it can be applied approximately to cases of irregular waves by considering the surge added mass and wave excitation force calculated at the peak frequency of the wave spectrum and estimating the surge hydrodynamic damping by means of the slope of the ship resistance curve at the given speed as follows:

$$b_{11} = \frac{dR_T(V_s)}{dV_s} = \frac{d(R + R_{AW})}{dV_s}. \qquad \text{Eq. 2}$$

Moreover, in the case of surge motion of the considered ships a_{11} is found to be negligible small and thus is omitted. In the case of very small ship surge oscillations $|\dot{\varsigma}_1| \ll V_s$ and small wave surge excitation $F_1 / R \ll 1$, a further simplification of the above dynamical model can be obtained by neglecting the fast time-scale effects involved in propeller hydrodynamics due to the viscous wake effects associated with the propeller operation in the wake of the ship, which permits the use of the steady open-water characteristics of the propeller in conjunction with appropriate tuneable coefficients estimated by unsteady propeller hydrodynamic analysis for the inclusion of the wave effects, as described in more detail the next subsection. For this purpose, we consider the following time-varying coefficient

$$\frac{K_T}{J^2} = \frac{(R + R_{AW} - T_{WASP})/N_p}{\rho(1-t)(1-w)^2 (U + \alpha u_w)^2 D^2} = C(t) \qquad \text{Eq. 3}$$

where K_T and K_Q, are the propeller thrust and torque coefficients $T_p = \rho n_p^2 D^4 K_T(J; C(t))$, $Q_p = \rho n_p^2 D^5 K_Q(J; C(t))$, $J = U/(nD)$ is the propeller advance ratio, where $U = (1-w)V_S$ and $1-w$ denotes the mean volumetric wake fraction on the propeller disc (defined as the mean value

of the axial propeller inflow), $n = \omega / 2\pi$ denotes the propeller revolutions per second (ω is the propeller angular velocity), and $D = 2R$ is the propeller diameter, respectively. In the above equation u_w denotes the wave velocity on the propeller disc and α denotes a tuneable coefficient that enables the incorporation of the effects of the propeller(s) oscillatory motion at the stern of the ship [6] which will be presented with more detail below.

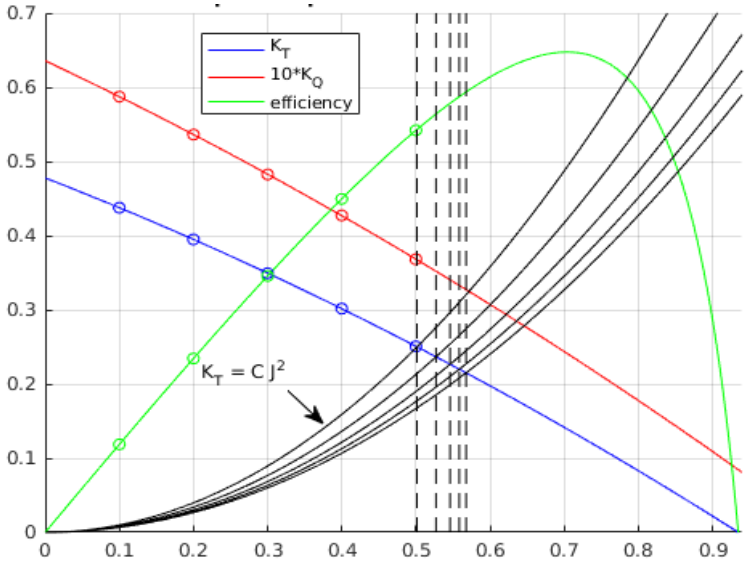

Figure 3: Propeller quasi-steady analysis based on K_T and K_Q , J propeller characteristics.

The temporary operation point of the propeller is obtained usually by fitting the parabolic curves $K_T = C(t)J^2$ to the propeller steady characteristics $K_T(J)$, as illustrated in Figure 3, from which the prediction of the propeller thrust, torque and the rotational speed are obtained as follows $T_p(t), Q_p(t), n_p(t) = (1-w)(U + \alpha u_w)/(JD)$, and finally the engine Shaft Horse Power is estimated as follows:

$$SHP = (Q_p \omega)/(\eta_R \eta_S) \qquad \text{Eq. 4}$$

where η_R is the relative rotative efficiency and η_S the shafting system efficiency.

3 Vortex Element Model for the unsteady analysis of propellers in waves

Assuming weak interaction between the propeller and the onset flow corresponding to the ship's wake, the unsteady propeller performance is treated in the framework of lifting flow applications, modelling the vorticity generated by the propeller blades by trailing vortex sheets. Except for the ship viscous wake generating unsteady propeller loads and responses, in the present model additional effects due to wave velocity and vertical oscillatory motion of the propeller(s) operating at the stern of the ship are also considered; see Figure 4.

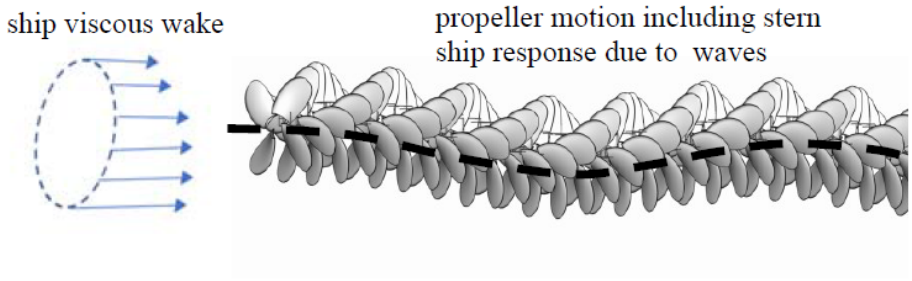

Figure 4: Unsteady propeller analysis including stern motion in waves.

The model is described in more detail in [6]. In particular the following representation is used to model the propeller disturbance velocity field:

$$\mathbf{u}(\mathbf{x}) = \frac{1}{4\pi}\int_{S_B \cup S_C} \frac{\sigma \mathbf{r}}{r^3} dS(\mathbf{x}_0) + \frac{1}{4\pi}\int_{S_B \cup S_W} \boldsymbol{\gamma} \times \frac{\mathbf{r}}{r^3} dS(\mathbf{x}_0), \qquad \text{Eq. 5}$$

where $\mathbf{r} = \mathbf{x} - \mathbf{x}_0$, σ is surface source-sink distribution on the blade S_B and cavity S_C surface, and $\boldsymbol{\gamma}$ the surface vorticity on the blade and trailing vortex surface S_W. The solution of the problem is obtained in the time domain by the enforcement of the no-entrance boundary condition on the propeller blades and solid surfaces in the propeller frame of reference,

$$\mathbf{n} \cdot \mathbf{u} = -\mathbf{n} \cdot \mathbf{q} \qquad \text{Eq. 6}$$

where the total fluid velocity $\mathbf{w}$ is given by:

$$\mathbf{w} = \mathbf{q} + \mathbf{u}, \quad \text{with incident flow } \mathbf{q} = \mathbf{U} + \boldsymbol{\omega} \times \mathbf{r} + \mathbf{v}_s, \qquad \text{Eq. 7}$$

with $\mathbf{U}$ and $\boldsymbol{\omega} \times \mathbf{r}$ denote the components due to propeller translational and rotational speed, respectively, and $\mathbf{v}_s = (u_s, v_s, w_s)$ represents the disturbance of the incoming flow to the propeller due to the ship's viscous wake and any other factors. In this work we consider as additional components the effect of wave velocities on the propeller plane, in conjunction with the vertical stern motion due to ship heaving and pitching in waves, in the ship frame of reference, see Figure 4.

The simulation of the propeller hydrodynamic performance in the spatially varying inflow conditions due to ship's wake is based on the Vortex Element Method [6]. The discretization consists of quadrilateral vortex element on the mean camber sufaces in conjunction with source-sink elements to model blade thickness and possible cavitation effects, as described in more detail in [9]. However,

in the present work propeller cavitation is not studied and is left for future extensions. In fact this is expected to be important particularly in cases of extreme responses in waves due to the proximity of propeller to the free surface.The numerical solution is obtained by a time-marching method where, at each time step, the velocity is computed from singularity distributions, and subsequently, the pressure is obtained from application of Bernoulli's equation appropriately modified to take into account propeller unsteady flow effects. The unsteady blade forces and moments, including the key blade thrust, $T_{,1}$, and torque, $Q_{,1}$, are calculated by pressure integration on propeller blades. For a specific mean value of the advance coefficient

$$J = U/(nD), \text{ where } U = (1-w)V_S \qquad \text{Eq. 8}$$

the blade thrust and torque coefficients are:

$$K_{t,1} = \frac{T_{,1}}{\rho n^2 D^4} \text{ and } K_{q,1} = \frac{Q_{,1}}{\rho n^2 D^5} \qquad \text{Eq. 9}$$

The corresponding propeller coefficients K_T and K_Q, are obtained by summation taking into account the contributions by all blades and the phase difference of the corresponding load histories.

As a verification example, we consider the case of propeller model N4118, for which experimental data are available (see, e.g. [10]). The basic dimensions of the above 3-bladed, unskewed propeller model with relatively thin blades are: diameter D=2R=0.3048m, pitch/diameter ratio P/D=1.077 (at 70% of tip radius), expanded area ratio 0.6, and the design value of the advance coefficient is J=0.833. The blade hub-tip ratio is 0.2, the blade section camber is NACA a08 and the thickness form NACA66MOD. The present model predictions concerning the open water characteristics of the above propeller model are shown in Figure 5 by using lines, together with experimental data shown by markers. Numerical predictions are obtained using a mesh of 15 x 7 elements on each blade in the spanwise and chordwise directions, respectively, depicted also in Figure 5.

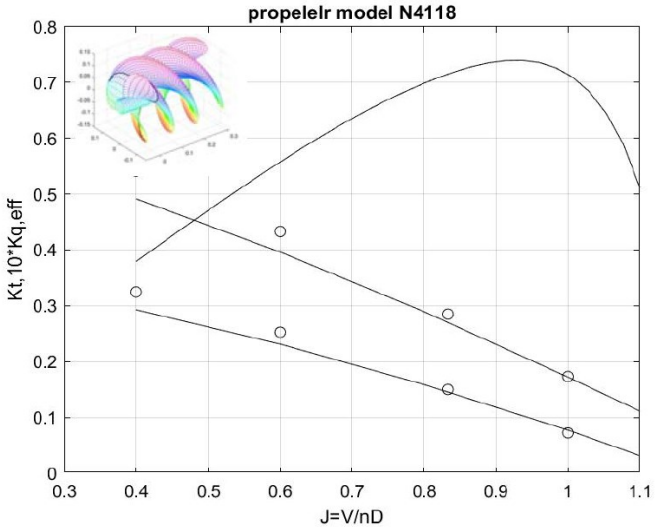

Figure 5: Open water characteristics of propeller N4118. Present model predictions are shown by using lines and experimental data by solid markers.

This mesh is shown to be enough for convergence in an interval around the operation (design) advance coefficient J=0.833, where the present model predictions agree well with experimental data. This is important for the unsteady propeller performance at this operation region of the propeller which will be discussed in the following. Differences appearing for smaller J-values corresponding to increased propeller loading conditions are mostly due to viscous flow separation effects, which could be better predicted by CFD viscous methods.

Next, the unsteady analysis of the propeller model is considered, concerning its performance in the axial wake flow shown in Figure 6. More specifically, the time-history of the thrust and torque coefficient of the key blade ($Kt_{,1}$ and $10Kq_{,1}$, respectively) are obtained from the unsteady hydrodynamic analysis of the propeller in non-cavitating conditions, for the design value of the advance coefficient J=0.833. In particular, the propeller operates in the axial onset flow corresponding to the axial onset flow on the propeller disc shown in Figure 6a as an angular distribution at various radial positions r/R=0.25,0.50,0.75, and the calculated blade thrust coefficient during one rotation is presented in Figure 6b. The present model predictions are obtained using the same as before blade mesh and a time-step corresponding to 6° propeller angular rotation. Calculations include also viscous corrections based on empirical sectional drag coefficient for $Re=10^6$ (corresponding to the conditions of experiments) from which the rotational speed of the propeller model is estimated as n=10.4RPS and the propeller forward speed Vs=2.64m/s.

Table 4: Responses of propeller model N4118.

	model 0 harmonic	**model 3 harmonic**	**experiment 0 harmonic**	**experiment 3 harmonic**
Kt	0.145	0.075	0.150	0.068
10*Kq*	0.270	0.125	0.285	0.110

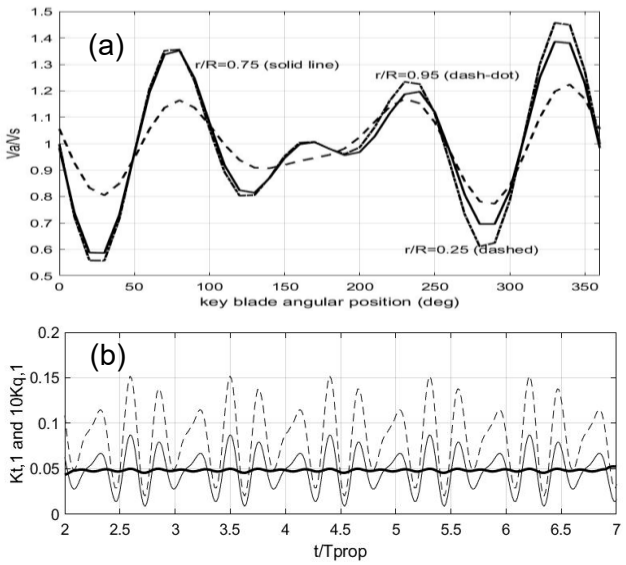

Figure 6: (a) Axial wake distribution on the propeller disc representing ship's viscous wake on the propeller disc of model N4118, for various blade radial positions during one revolution. (b) Calculated time-history of the blade thrust Kt,1 (solid line) and torque 10Kq,1 (dashed line) coefficients of the key blade during 5 revolutions, operating in the ship's wake. The low frequency oscillation of the thrust response induced by considering the additional wave effects is shown using thick lines.

In this case the comparison between calculated and measured data related to the mean propeller responses and the amplitude of the first blade harmonic is presented in Table 4. It is seen that the present numerical method provides good predictions, especially for the mean propeller thrust and torque. Moreover it leads to an overprediction of the blade frequency harmonics which is considered to be within acceptable limits with regard to the examined case characterized by quite strong inhomogeneity of the axial onset flow. Application of the present Vortex Element Model to other *J* values around the design point *J*=0.833 of propeller model N4118, provides the calculation of the mean K_t *and* K_q characteristics, as shown in Figure 5, from which the estimation of the derivative $\left[dK_t/dJ\right]_{J=0.833} \approx -0.45$ is obtained.

Next, we will consider the problem of simulating the flow around a propeller undergoing more general motion. This will include the effect of the oscillatory vertical stern motion of the ship travelling in waves, while operating in the ship's viscous wake. The same propeller is considered operating in the same as before conditions including a disturbance flow component due to waves and vertical oscillation of the propeller. The instantaneous orientation of the axes of the body-fixed frame of reference, described by the rotation angles $\left(\theta(t),\psi(t),\chi(t)\right)$.

A general path defined by the propeller advance with the ship (steady translation motion), in conjunction with the induced vertical stern motion of the propeller simulating stern ship in waves is considered, as e.g., predicted by seakeeping analysis; see also Figure 4. The propeller is assumed to steadily rotate with angular velocity $\omega = 2\pi n$ (where *n* denotes the revolutions per second) and simultaneously performing heaving oscillation, due to the motion of the ship in waves. Therefore, in the examined case we consider the following motion variables (where *L* is representative of the ship length):

$X(t) = V_S t$, $Y(t) = 0$, $Z(t) =$ vertical stern motion

$\theta(t) = \omega t$, $\psi(t) = \tan^{-1}\left(2Z(t)/L\right)$, $\chi(t) = 0$.

Indicative results are presented in Figure 7 for propeller model N4118 operating at *J*=0.833, in the same as above conditions and in the axial flow simulating ship's wake distribution of Figure 6. Except

for the axial wake effect, also the oscillatory component of the horizontal wave velocity component on the propeller disc and the vertical oscillatory motion of the propeller due to waves are taken into account, while assuming small effect of ship pitch, i.e. $\psi(t) \approx 0$. For simplicity, we consider harmonic waves of period $2\pi/\omega_w$=0.7sec, where ω_w is the wave frequency in the inertial frame of reference, and its amplitude A=0.1R. Thus, the horizontal wave velocity on the propeller disc is

$$u_s(t) = -(gAk/\omega_w)\exp(-kd)\sin(\omega_e t) \qquad \text{Eq. 10}$$

where d stands for the propeller submergence depth, $k = \omega_w^2/g$ is the deep-water wavenumber, and $\omega_e = \omega_w + kV_s$ denotes the encounter frequency in the case of head waves. Moreover, the velocity due to the vertical motion of the propeller, assuming the same amplitude A, is

$$w_s(t) = -\omega_e A\cos(\omega_e t) \qquad \text{Eq. 11}$$

The above components are illustrated in Figure 7a, in a time interval equal to 5 propeller revolutions, using solid and dashed lines, respectively. The calculated time histories of key blade thrust, and torque are plotted in Figure 7b, as obtained by the present Vortex Element Method. It is clearly observed that the variation of blade thrust and torque $Kt_{,1}$ and $Kq_{,1}$ is affected by the additional wave induced components $u_s(t)$ and $w_s(t)$. This effect is furthermore illustrated in Figure 8 concerning the thrust coefficient of the propeller (obtained by the contribution of all unsteady blade loads) operating at J=0.883 in the wake of Figure 6a, where the low frequency of oscillatory thrust response due to waves is also plotted by shown by using thick solid line. The observed rapid thrust fluctuations correspond to the blade harmonic frequency due to the ship viscous-wake effects (solid lines), and the dashed lines indicate the low frequency oscillation of the propeller thrust response due to the wave effects.

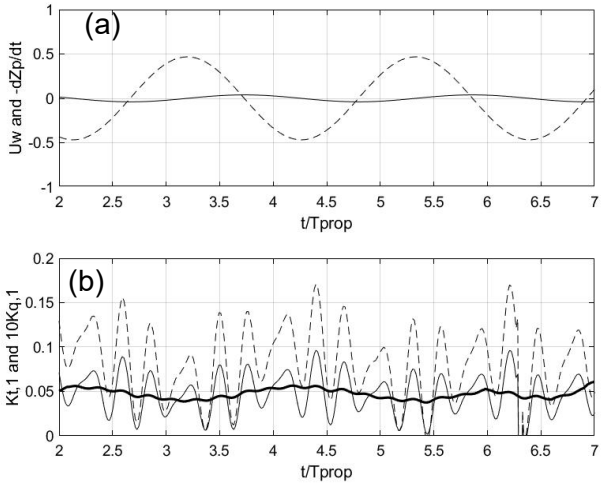

Figure 7: (a) Harmonic wave axial velocity (solid line) and velocity due to vertical propeller motion (dashed line). (b) Calculated time-history of the key blade thrust Kt,1 (thin solid line) and torque 10Kq,1 (dashed line) coefficients of propeller N4118 during 5 revolutions, with the additional effect of waves. The low frequency oscillation of the thrust response induced by considering the additional wave effects is shown using thick lines.

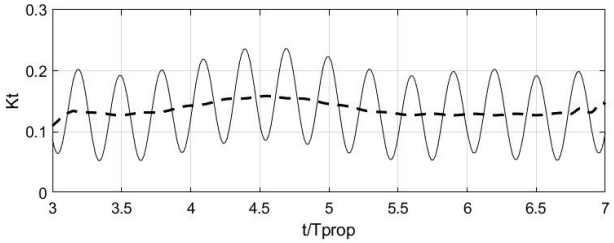

Figure 8: Total response concerning the thrust coefficient of the propeller N4118 in the wake of Figure 6 with the wave effects. The low frequency propeller response is shown by using dashed lines.

From Figure 8 we obtain that the amplitude of the low frequency response due to waves is about 10% of the mean thrust value, and the corresponding thrust coefficient of the propeller takes values in the interval $K_t = 0.145 \pm 0.015$. This analysis can be extended to take into account the extra terms (Eq. 11 and Eq. 12) associated with the propeller oscillation in wave conditions characterized by a frequency spectrum using the ship responses; see also [8], [11].

Assuming that the two wave induced effects on the propeller performance due to $u_s(t)$ and $w_s(t)$ contribute equally to the low-frequency oscillation of the propeller response in waves, the prediction of the wave and ship-response effects on the propulsion performance can be based on the quasi-steady approximation. In the example considered above related to the propeller N4118, the variation of the advance coefficient due to the horizontal wave orbital velocity has been calculated from Eq.(10) to be : $\delta J = |\delta u_s| / U = 0.015$, and the amplitude of variation of the propeller thrust using the open-water characteristics of Figure 5 is estimated to be: $\delta Kt = [dKt/dJ]_{J=0.833}\, \delta J \approx \pm 0.007$. Comparing the latter value with the thrust variations derived by the unsteady propeller analysis in waves using the Vortex Element Method (see also Figure 8), an estimation of the coefficient $\alpha = 2$ can be suggested for the specific case. Appropriate values for the α-coefficient, in the interval $\alpha = 1 \div 2$, are dependent on the wave conditions. The value of the coefficient $\alpha(H_S, T_P)$ could be estimated for other configurations and wave conditions by application of the present method to several sea states, represented by the significant wave height H_S and peak period T_P of the corresponding frequency wave spectrum and the ship responses.

4 Application to the case of the BC ship MV Kastor

In the following, the case of the Bulk Carrier MV Kastor of DWT82000 at scantling draft Td=14.45m will be examined and predictions of the propulsion performance in waves based on the developed simplified approach will be shown and discussed, illustrating the applicability of the present model in realistic cases. Main dimensions of the BC ship and details are provided in Appendix A.

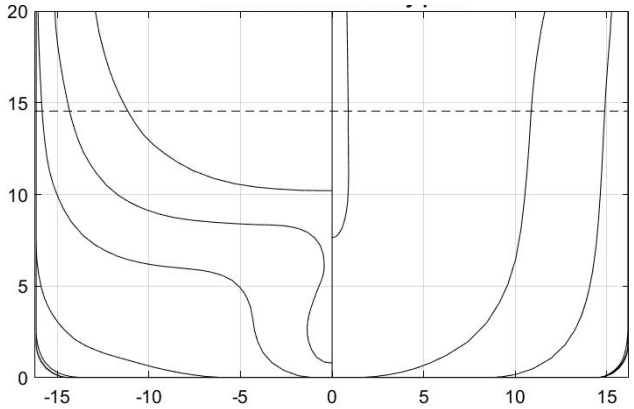

Figure 9: Body plan of the BC hull studied with main dimensions: length L=229m, breadth B=32.28m, and deck height D_h=20m. The scantling draft T_d=14.45m is indicated by using a dashed line.

4.1 Ship and propeller data

The body plan of the ship is presented in Figure 9. The dimensions of the ship are: Length L=229m, Breadth B=32.28m, Deck height D=20m (from keel). The scantling draft is T_d=14.45m, and in the full load condition the ship is without trim, with a representative value of the block coefficient of Cb=0.86.

Moreover, the static stability diagram of the ship, for the full loading condition T_d=14.45m, based on the value of KG=11m for the vertical centre of gravity (measured from keel) is presented in Figure 10. Since the ship in full load condition is considered without trim, the longitudinal center of gravity coincides with the longitudinal center of buoyancy (LCG=LCB=3.34m) forward the midship section. Also, using an estimation for the vertical center of buoyancy KB=7.55m and the metacentric radius BM=6.24m, the metacentric height for T_d=14.45m is GM=2.79m, as it is also indicated in Figure 10 using a dashed line.

The ship is equipped with a Diesel main engine with MCR 9930 kW at 90.4 rpm, which is directly coupled to the propeller, and the shafting system efficiency is estimated to be 98%. Also, from the analysis of operational data as presented in D3.1 [7], time instances corresponding to the examined loading conditions and a ship's speed range Vs= 9-15kn are identified

Available data from towing tank resistance in calm-water (in kN) covering this speed range are included in the last row of

Table 5. In addition, data are available for the wake fraction 1-w=0.36, the thrust deduction factor 1-t=0.25, and the relative rotative efficiency η_R=1.006, as obtained from model tank tests in the full load condition of the examined ship without trim. Data for the additional impact of the vertical ship motion on the installed ESDs were not available and not examined here. The latter are expected to be much less relevant than the effects of the vertical stern motion which is the focus of the present study.

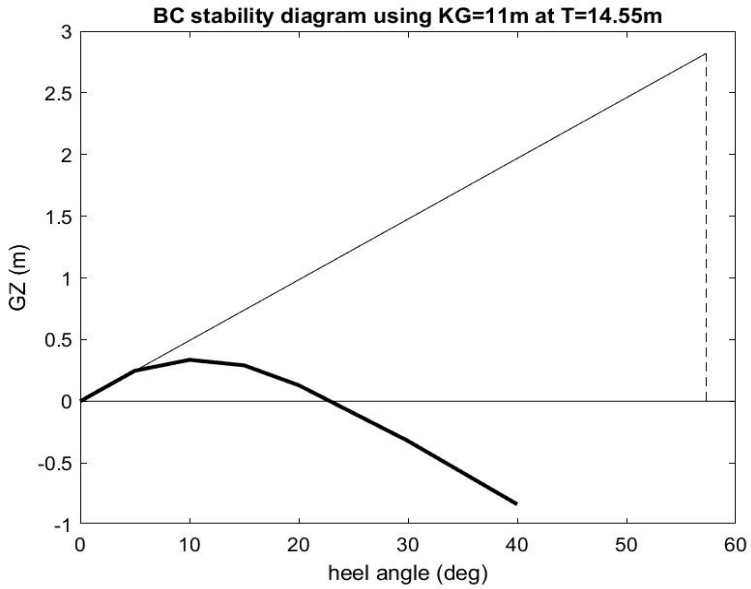

Figure 10: Stability diagram of BC for the scantling draft T_d=14.45m based on KG=11m from keel.

Table 5: Resistance [kN] of the BC hull for draft T_d=14.45m.

U[kn] / Sea state	10	12	13	14
1	0.5	0.2	0.1	0.1
2	9.6	7.0	6.0	5.4
3	51.3	42.2	38.4	35.1
4	160.8	149.1	143.4	138.8
5	342.8	344.9	345.8	344.1
R_{CW}	342.80	501.44	605.82	727.00

The studied BC is equipped with a 5-bladed propeller of diameter D=6.95m, with expanded area ratio Ae=52% and pitch-to-diameter ratio P/D=0.77. The specific propeller geometry has been reconstructed using limited information from drawings and BC ship reports and 3D models have been developed by NTUA in Rhino© and used for hydrodynamic analysis using VLM, BEM and CFD. The open water characteristics of the propeller calculated by the present VLM and BEM using the mesh shown in Figure 11 are presented in Figure 12 by using solid lines, and compared with results from CFD analysis for verification, which are shown in the same figure with markers.

On the basis of the preceding analysis the predicted behaviour of the propulsion system of the BC ship in calm water is presented in Figure 13. Results are obtained using the calm-water resistance R_{CW} from model tank tests (

Table 5 (last row)). In particular, the calculated performance of the propulsion system is shown on the main engine SHP-RPM diagram in Figure 13a (red line) and the corresponding ship speed Vs-RPM data are presented in Figure 13b (black line). Based on Figure 13 for the maximum engine speed of 90.4 RPM, we obtain Vs=14.54kn and SHP=8630 kW, with a margin of 13% relatively to the MCR.

In the same plots in Figure 13a and Figure 13b the ship operational data are also shown using markers. The latter data are fitted, and the results are shown by using dashed blue lines, indicating on average a difference in ship speed by approximately 1kn, which could be due to possible effects

of currents, and an increase in SHP by 9%, which could be due to weather conditions and other effects.

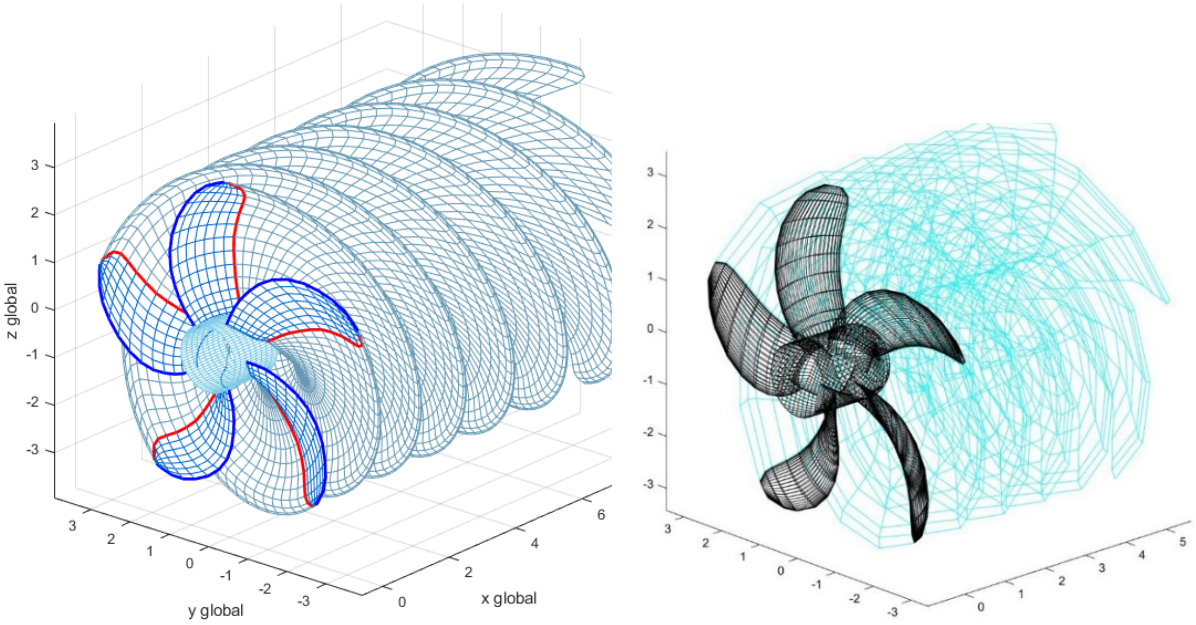

Figure 11: (Left) Vortex Element Model used for the BC propeller analysis with a discretization of 15 spanwise by 7 chordwise elements per blade. (Right) BEM analysis using finer discretization

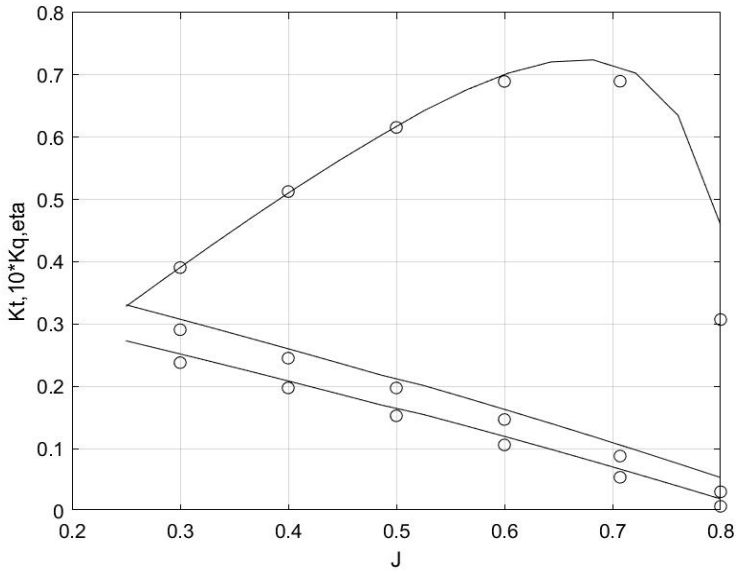

Figure 12: Open water characteristics of the BC propeller of Figure 11, as obtained by the present vortex element model using a discretization of 15 spanwise by 7 chordwise elements per blade. Results from CFD verifying model predictions are indicated by using markers.

The predictions have been obtained by using the present model, in conjunction with calm-water resistance data and hydrodynamic hull- propeller interaction coefficients, obtained from model tank self-propulsion tests.

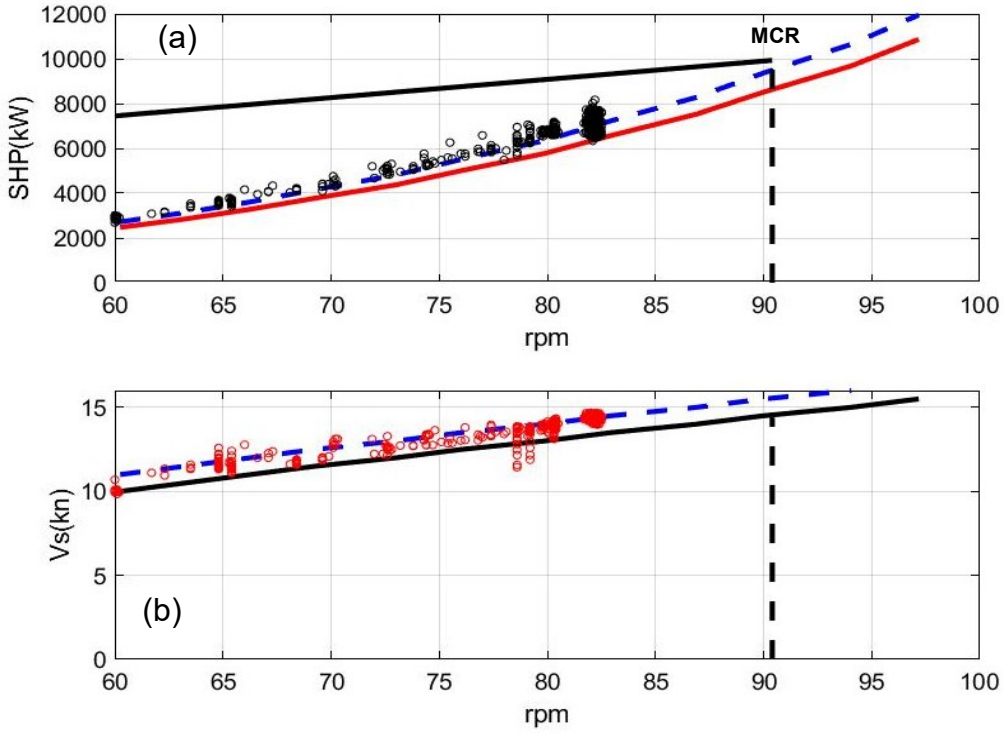

Figure 13: Behaviour of the propulsion system based on the calm-water resistance characteristics based on tank model data for the BC ship corresponding to full-load draft T_d =14.45m without trim (shown by using solid line). (a) SHP-RPM diagram and (b) Ship speed - RPM diagram.

4.2 Seakeeping analysis

An important factor related to ship operation in realistic sea-states, strongly connected also to ship dynamics, is the added resistance in waves. This could also have an important effect on the economical ship exploitation.

In several works (see, e.g. [12]), several available methods concerning the estimation of added wave resistance are studied and validated against seakeeping tests of monohull models, focusing on head seas, which is usually the most severe situation for the added wave resistance. The analysis shows that radiated energy methods (see [13]) could provide relatively good quality results in many cases. In the present study we employ the radiated energy method, as extended by [14] for the prediction of head-to-beam seas, in conjunction with strip theory [15] for the calculation of the added resistance and the vertical ship motion at the stern using the Frank close-fit method (see also [16]).

Numerical results obtained for the responses of the BC hull studied are presented in Figure 14, for ship speed Vs=14kn, at full load draft without trim. In particular, the calculated RAO (modulus and phase) of heave and pitch motion are plotted vs the non-dimensional wavelength (λ/L). For the same condition and ship speed, the calculated response regarding the added wave resistance R_{AW} is plotted in Figure 15, for head incident waves β=180°, where the calculated coefficient $WAR = R_{AW} / \left(\rho g A^2 B^2 / L \right)$ is shown, with A denoting the wave amplitude, and L, B are the ship length and breadth, respectively.

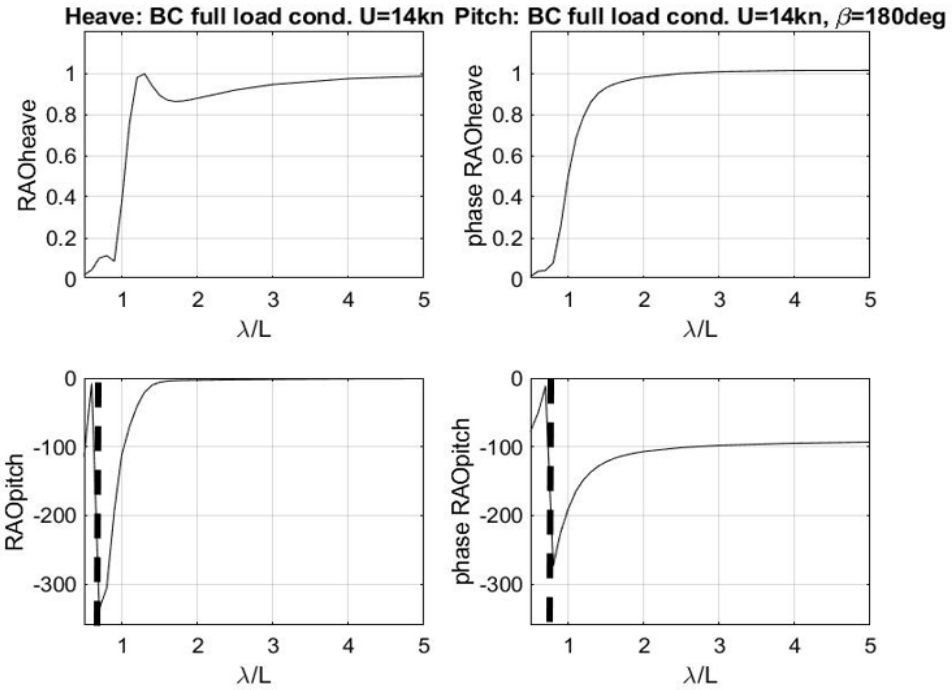

Figure 14: RAO (modulus and phase) of BC hull heave and pitch responses for Vs=14kn (F=0.15) against the non-dimensional wavelength (λ/L) for the full load condition (T_d=14.45m, without trim).

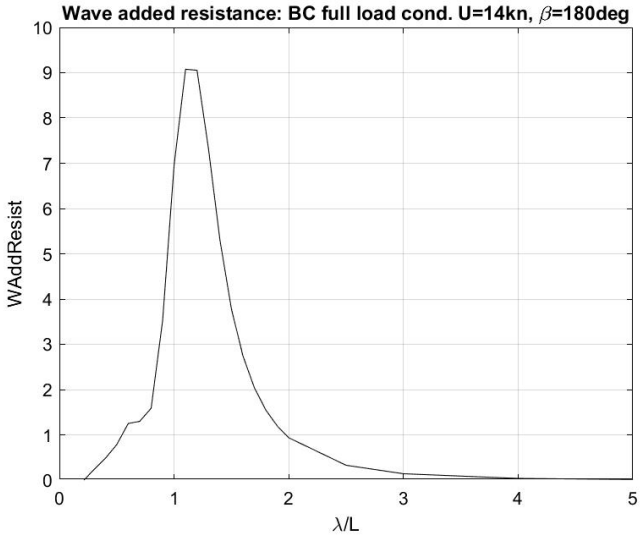

Figure 15: Calculated added wave resistance for the BC at full loading condition T_d=14.55m, V_S=14kn (F=0.15), and head incident waves β=180°.

The results for the calculated mean wave added resistance of the studied BC ship in different sea-states are listed in

Table 5 for various ship speeds in the range 10 – 14kn, corresponding to Froude numbers *Fr*=0.11-0.15, respectively, in head waves (β=180°). In the case of irregular waves, we consider the responses of the system operating at various sea conditions labelled by a sea-state index ranging

from 1 to 5, corresponding to values of the significant wave height and modal period as listed in Table 6.

Table 6: Significant wave height and modal period for various sea states using the Bretschneider spectrum model.

Sea state	2	3	4	5	6
H_s[m]	0.3	0.9	1.9	3.3	5
T_p[s]	6.3	7.5	8.8	9.7	12.4

For the calculations the Bretschneider wave spectrum is used, which is expressed as

$$S(\omega\ ) = \frac{1.25}{4}\frac{\omega_p^4}{\omega^5}H_s^2\, exp\left(-1.25\frac{\omega_p^4}{\omega^4}\right), \qquad \text{Eq. 12}$$

where the modal (peak) period $T_p = 2\pi / \omega_p$ for various sea-states with the index corresponding to values of the significant wave height and period as provided in Table 6. A representative plot of the wave spectrum for H_S =3.3m and T_p =9.7s (sea-state 5) is shown in Figure 16.

The corresponding frequency of encounter ω_e is given by:

$$\omega_e = \left|\omega\ - \left(\omega^2 / g\right)V_S \cos\beta\right| \qquad \text{Eq. 13}$$

in terms of the absolute wave frequency ω, the ship's speed V_S and mean wave direction β. From the above equations (12,13) the spectral density in terms of encounter frequency is obtained as follows,

$$S\left(\omega_e\right) = S\left(\omega\right)\left(1 - 2\left(\omega V_S / g\right)\cos\beta\right)^{-1} \qquad \text{Eq. 14}$$

where the Bretschneider spectrum (Eq. 12) is used for $S\left(\omega; H_S, T_p\right)$.

Using standard methods the spectra of various quantities (i.e., wave velocity etc) can be calculated, and short-term time series simulations, with reference to a particular sea state $(H_S, T_P; b)$ are obtained by considering the processes to be stationary and characterized by a narrow band spectrum of the response(s). For example, in the case of horizontal wave velocity on the propeller:

$$S_U\left(\omega\right) = \int_\theta \left|RAO_U\left(\omega_e, \theta\right)\right|^2 S\left(\omega_e, \theta; H_S, T_p, \beta\right) d\theta \qquad \text{Eq. 15}$$

with $RAO_U\left(\omega_e, \theta\right) = \omega\left(\omega_e\right)\exp\left(-d\omega^2\left(\omega_e\right)/g\right)$ and d is the propeller submergence depth. The stochastic simulation of wave velocities in the propeller plane is similarly treated.

For simplicity, in the present study the wave spectrum is modelled as a unidirectional one, i.e. $S = S(\omega_e; H_S, T_p)\delta(\theta - \beta)$, representing long-crested seas. Subsequently, the random phase model (see e.g. [17]) is applied to obtain a short-term time series of horizontal wave velocity on the propeller plane, as follows:

$$u_w(t) = \sum_{n=1}^{N} U_n \cos(\omega_{e,n} t + \varepsilon_n), \qquad \text{Eq. 16}$$

where e_n are random variables uniformly distributed in [0,2π). The horizontal wave velocity amplitudes are given by $U_n = \sqrt{2S_U(\omega_n)\delta\omega_n}$ and the set of discrete encounter frequencies $\{\omega_{e,n}\}$ are appropriately selected to cover the essential support of the spectra and to represent well the energy distribution around the peak frequency.

Similarly, the free surface elevation is modelled using the above random phase model as follows:

$$\zeta(t) = \sum_{n=1}^{N} A_n \cos(\omega_{e,n} t + \varepsilon_n), \text{ with } A_n = \sqrt{2S(\omega_{e,n})\delta\omega_n}, \qquad \text{Eq. 17}$$

where the wave frequency spectrum for sea condition 5, using the Bretschneider model, is illustrated in Figure 16.

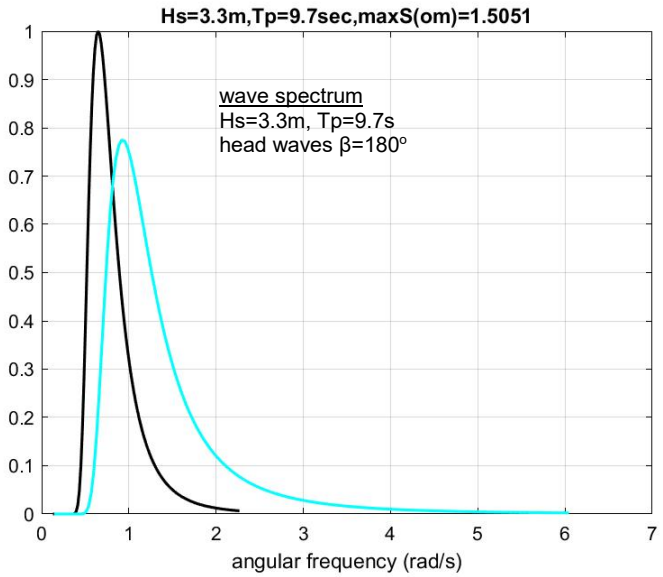

Figure 16: Wave frequency spectrum S(ω) for sea condition 5, using the Bretschneider model, normalized by its peak value. The same spectrum vs the encounter frequency for *V*s=14kn is plotted by using cyan line.

4.3 Performance prediction based on the dynamical system

Indicative results concerning the free-surface elevation and the horizontal wave velocity time series for the BC ship, travelling at speed of Vs=14kn, in head waves at sea condition 5, are shown in the

two panels on top in Figure 17. More specifically in Figure 17a the free-surface elevation and in Figure 17b the horizontal wave velocity on the propeller plane $u_w(t)$ are shown using black lines.

In addition, the total axial flow velocity on the propeller $U+u_w(t)$ is plotted in in Figure 17b in red lines. The dynamic simulation of the propulsion system response in waves results in the SHP (kW) and the engine RPM shown in in Figure 17c and in Figure 17d, respectively. Moreover, the predicted results of the propulsion performance by the present dynamical model are shown in the last two subplots, obtained for $\alpha = 2$. In this case the average SHP indicated by the red dashed line in Figure 17c is 8870kW, which is 3% greater than the corresponding value in calm water. The average RPM is of 91.8. It is also observed that the peaks in the SHP and RPM time series exceed the MCR limit of the engine by 15%. This discrepancy could be reduced by incorporating damping effects in the system, for example by reducing the value of the α-coefficient, as illustrated and discussed below.

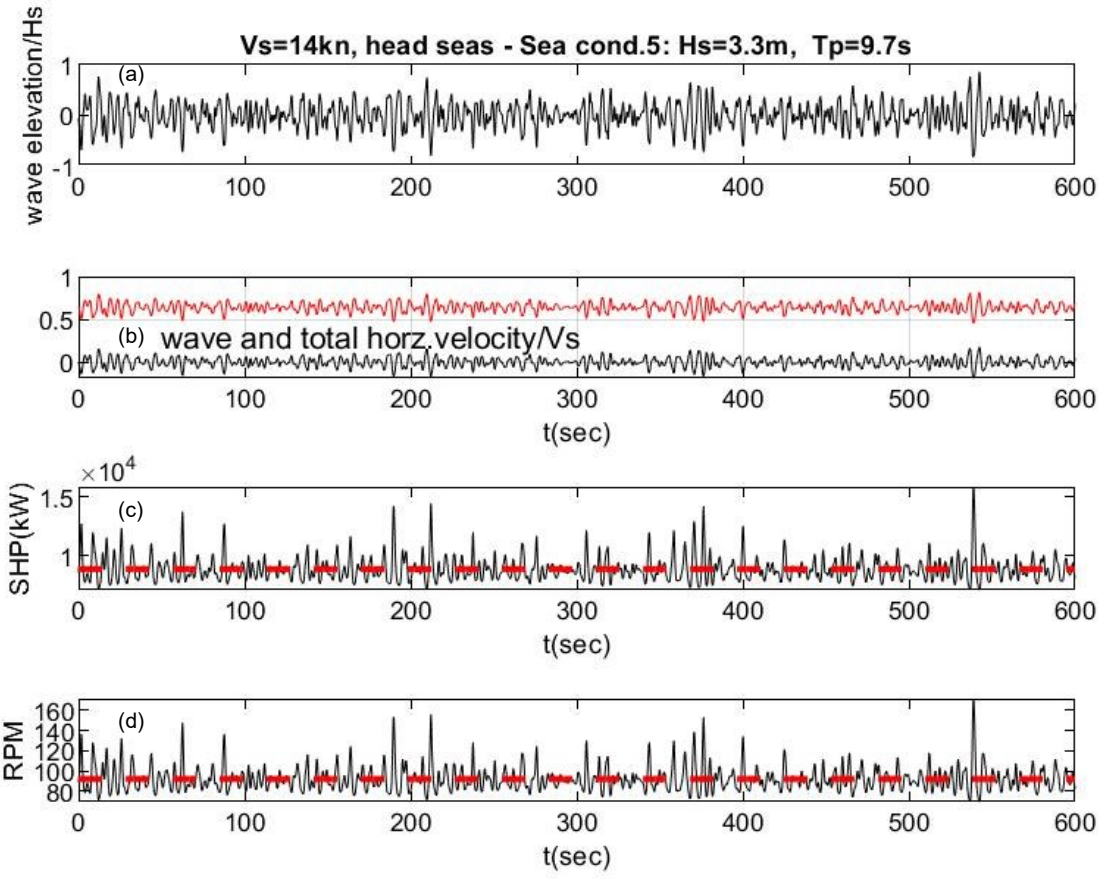

Figure 17: Simulated time series of ship performance in waves in a time scale of 10 minutes using α=2: (a) free-surface elevation and (b) horizontal wave velocity for the studied BC ship at full draft, travelling at speed of *V*s=14kn (F=0.15) in head waves at sea condition 5. Dynamic simulation of propulsion system response concerning (c) SHP (kW) and (d) engine rpm with corresponding mean values SHP=8880kW and RPM=89 indicated using red dashed lines.

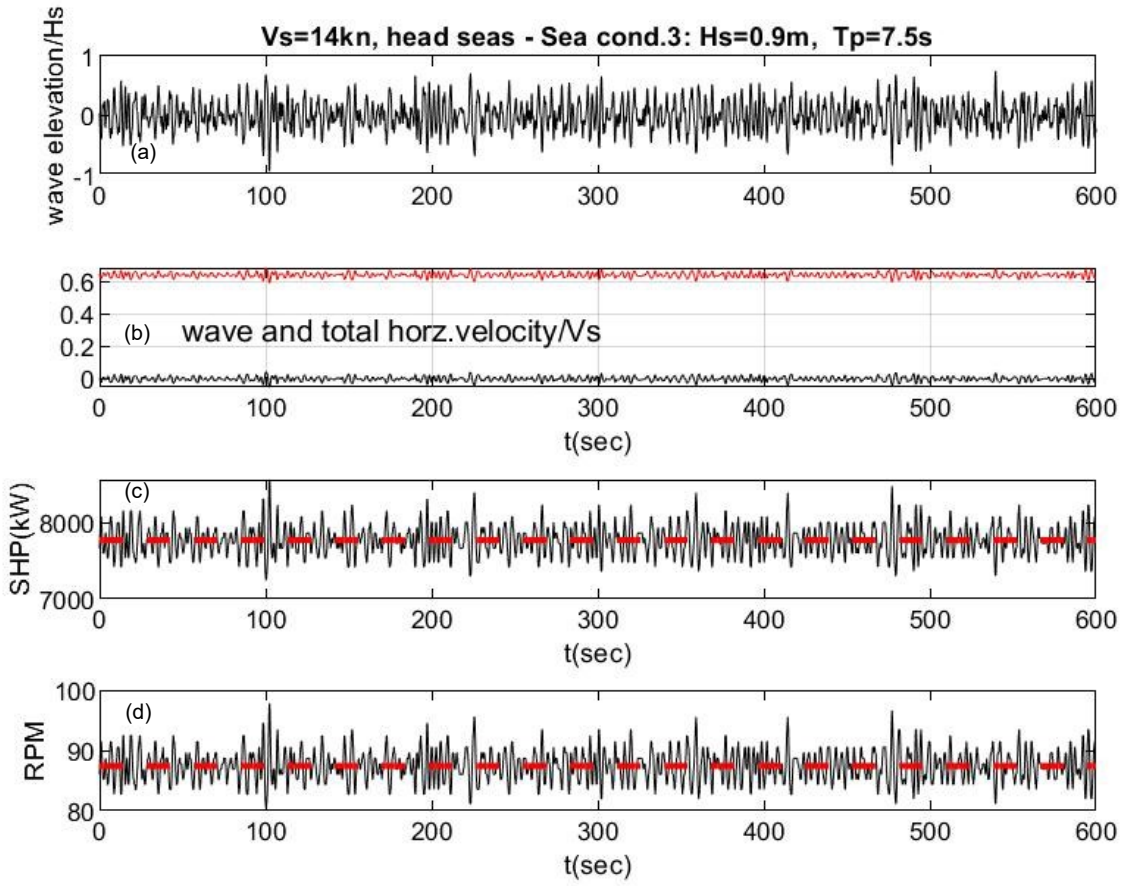

Figure 18: Simulated time series of ship performance in waves in a time scale of 10 minutes using α=1: (a) free-surface elevation and (b) horizontal wave velocity for the studied BC ship at full draft, travelling at speed of *V*s=14kn (F=0.15) in head waves at sea condition 3. Dynamic simulation of propulsion system response concerning (c) SHP (kW) and (d) engine RPM with corresponding mean values SHP=7768kW and RPM=87.43 indicated using red dashed lines.

The same analysis performed at α=1 for the ship at full draft, travelling at speed of Vs=14kn (F=0.15) in head waves at sea condition 3 (Hs=0.9m and Tp=7.5s) is shown in Figure 18. It is observed in this case that the average SHP indicated by the red dashed line in Figure 18c is 7768kW and the average RPM is 87.4. In this case the peaks in the SHP time series remain within the engine limits.

For the same two cases in Figure 19 and Figure 20, respectively, the effect of the α-coefficient on the numerical predictions by the present dynamical performance model of the ship travelling with speed Vs=14kn at sea conditions 5 and 3 is shown. The results are presented in a time scale of 50s, and the time variations associated with the wave effect at a representative time interval close to the period corresponding to the peak encounter frequency can be observed. In the third and fourth subplots of Figure 19 and Figure 20 the damping effect of the α-coefficient is clearly observed. More specifically, predictions based on α=2 are shown by using black lines and for α=1 using cyan lines, respectively. A reduction in the amplitudes of the rapid fluctuation of the engine performance is observed.

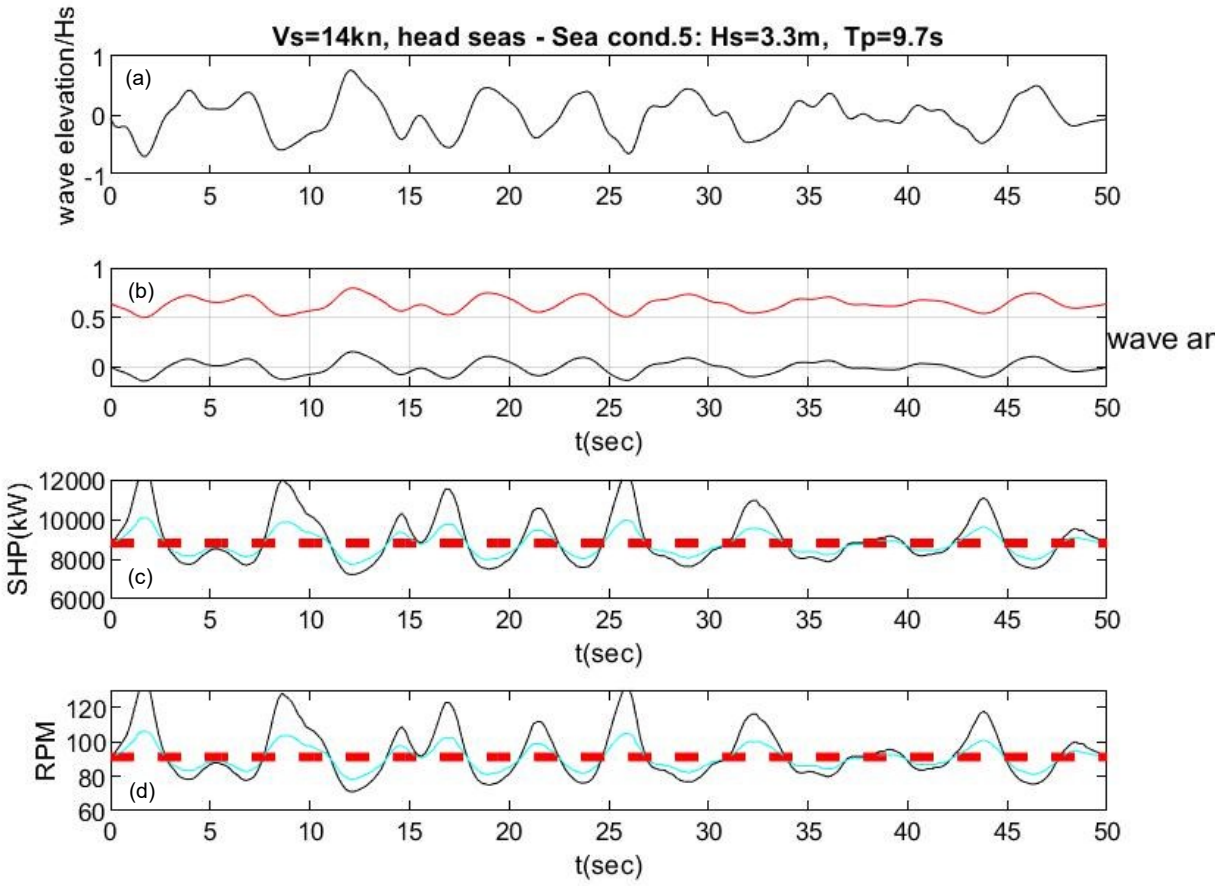

Figure 19: Same as in Figure 17 for the ship performance in a time scale of 50 sec for the studied BC ship at full draft, travelling at speed of *V*s=14kn (F=0.15) in head waves at sea condition 5. The effect of α-coefficient is shown in the last 2 subplots by using black lines (α=2) and cyan lines (α=1), respectively. Time average values are indicated using thick dashed lines.

The present analysis facilitates the rapid calculation of the effects of different sea conditions, as they are represented by weather predictions at scale of 10min intervals for example. Such an analysis could support a framework related to weather routing optimisation.

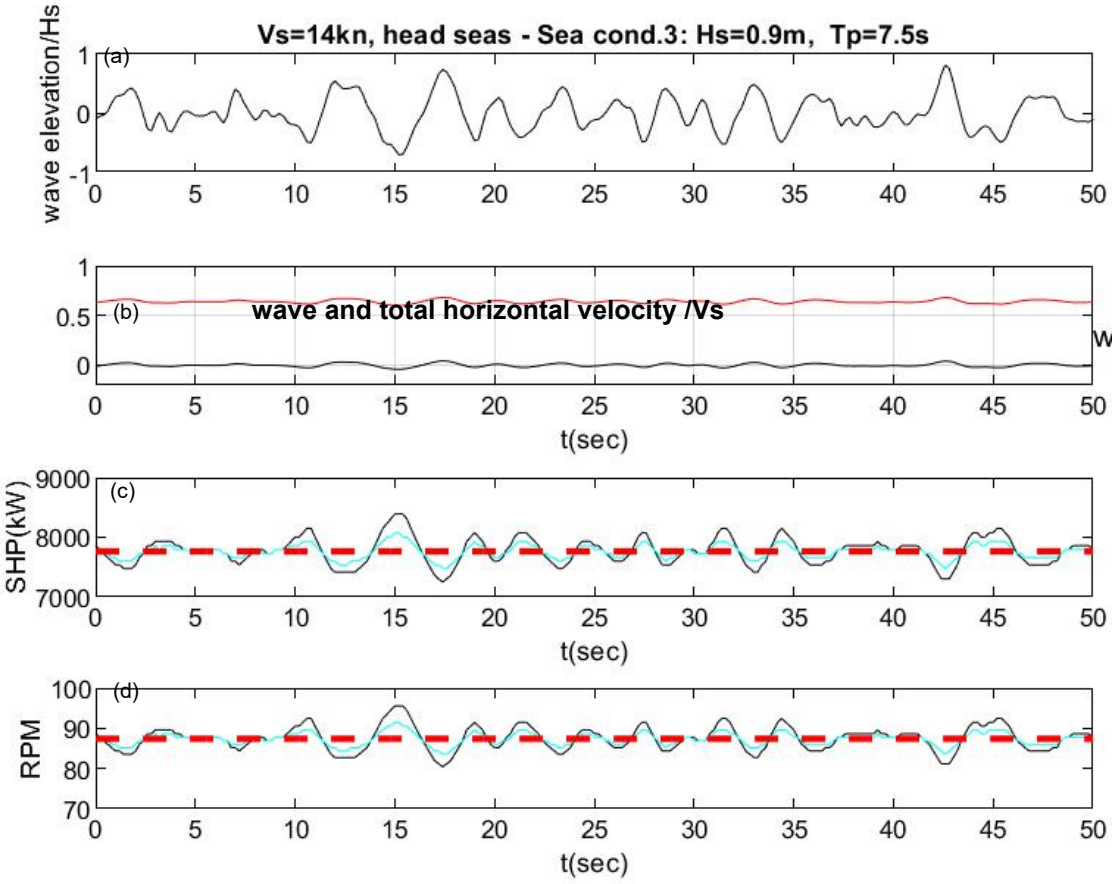

Figure 20: Same as in Figure 18 for the ship performance in a time scale of 50 sec for the studied BC ship at full draft, travelling at speed of *V*s=14kn (F=0.15) in head waves at sea condition 3. The effect of α-coefficient is shown in the last 2 subplots by using black lines (α=2) and cyan lines (α=1), respectively.

4.4 Analysis of the α-parameter effect on the operational performance

In this section the results obtained from the parametric analysis of a series of values for the α-parameter are presented, to investigate the effects of this tunable parameter on the performance of the propulsion system of the BC, across a set of operational and weather conditions.

Two different loading conditions are examined, namely the full load departure (R1445000- Case 1) and the laden condition (R1300050- Case 6), see Appendix A. Three different forward speeds of advance are investigated, covering the range 10-13 knots. The wave headings cover all directions from head (180°) to following (0°) seas with an increment of 30°, considering irregular sea state conditions 4 (Hs=1.90m/ Tp=8.80sec) and 5 (Hs=3.30m/ Tp=9.70sec). Three different values for the α-parameter are used, namely 0.75, 1.00 and 1.25, for a parametric analysis of the time-varying propeller loading. This loading is caused by the horizontal components of the wave velocity inside the propeller wake and the vertical motions of the propeller due to the ship's dynamic response in the seaway. The results obtained for Case 1 are presented in this section, while the calculations referring to Case 6 are given in Appendix C.

The results presented refer to the mean SHP and RPM values and the corresponding standard deviation, obtained from the SHP and RPM time history (e.g. Figure 17). The results are organized into figure groups corresponding to the same loading condition, sea-state and forward speed of advance. For each combination, bar charts for each α-parameter value and wave heading are plotted together. The different α values correspond to different colors on the bar charts that depict the mean values, while the slender black bar on top of each bar corresponds to the standard deviation.

To begin with the full load departure condition (R1445000-Case1), the results for the different speeds and sea states are presented in Figure 21 to Figure 32. Starting from the general remarks, the anticipated behavior regarding the increase in the SHP and RPM as the ship speed increases is clearly observed. Furthermore, it is observed that for a constant speed and considering following to beam wave directions, the SHP and RPM remain almost constant, while for oblique by the bow to head sea directions there is a general increase both to the SHP and the engine speed, with the peak appearing at 150° heading, namely 30° off-bow direction. This behavior is attributed to the fact that usually when a ship encounters waves in an off-bow direction of less than 45°, the contribution both due to the motions of the ship (radiated waves) and the diffraction are significant, leading to an increase of the added wave resistance, compared to other wave directions. This trend is observed for all examined sea states and forward speeds of advance.

With a comparative analysis of the effect of the α-parameter on the results for the sea-state 4 (Figure 21-Figure 26), it can be observed that the increase of α leads to an increase in the standard deviation, as indicated by the black slender bars in the graphs. This behavior is justified, since the α-parameter controls the intensity of the wave-induced disturbance of the wake flow at the propeller disk and consequently affects the propeller loading. As shown for example in Figure 19, a higher α-parameter value leads to more pronounced peaks in the SHP and RPM time-series, which in turn leads to a higher standard deviation. Moreover, it seems that the variation of the α-factor has negligible impact on the mean values of the SHP and RPM, for the same wave heading and vessel speed. Notably, for beam seas of 90° the same mean values and zero standard deviation is obtained, due to the fact that in this case the horizontal velocity of the wave is travelling tangentially to the propeller disk and therefore, theoretically the wake is not affected by the wave velocity.

Based on the calculations regarding sea-state 4 and comparing the SHP for the same wave direction and different speeds, it is shown that the increase of the power demand with increasing ship speed, leads also to higher SHP standard deviation. For example, for the peak power demand occurring at 150° wave direction, the results obtained for different α-parameters and vessel speeds, considering a sea-state 4, are summarized in Table 7 and Table 8. The tabular format is used for the discussion of the results, giving the percentage change of a quantity with increasing α and fixed ship speed (column-wise) or increasing ship speed with fixed α (row-wise). It can be observed that for a fixed vessel speed (e.g. 10kn) and varying α, the mean SHP remains essentially constant, while the SHP standard deviation changes by about 30% for α=1 and 70% for α=1.25, with reference to α=0.75. For a fixed α value (e.g. 0.75) an increase of the vessel speed leads to higher mean SHP by 47% for 11.5kn and 117% for 13kn, with reference to 10kn. The change of speed leads to an increase of the SHP standard deviation by 25-27% for 11.5kn and 63-69% for 13kn, with lower values corresponding to higher α. Regarding the behavior of the RPM mean value and standard deviation for a fixed speed and varying α, a similar trend as for the SHP is captured. The increase of ship speed to 11.5kn and 13kn, leads to an increase of the mean RPM by 14% and 30%, respectively, while the standard deviation is almost constant with a maximum change of about 2.2%. It has to be noted that the standard deviation value is more sensitive to the random phase difference associated

with the incoming irregular waves and a definitive trend regarding the change of the STD with increasing vessel speed cannot be established.

In Figure 27 to Figure 32 the results obtained for the heavier sea-state 5 are shown. The mean values of SHP and RPM are increased compared to sea-state 4, due to the increase of the wave added resistance. Based on the results for 150° wave direction, summarized in Table 9 and Table 10, it appears that the standard deviation for the SHP almost triples, while the standard deviation in RPM is increased by approximately 75% compared to sea-state 4.

Table 7: Variation of SHP mean value and standard deviation for 150° wave heading and sea state 4.

Mean SHP (150°)	**10 kn**	**11.5kn**	**13kn**	**11.5kn[%]**	**13kn[%]**
α=0.75	3018.17	4445.67	6557.88	47.30%	117.28%
α=1.00	3019.82	4447.45	6560.25	47.28%	117.24%
α=1.25	3022.28	4450.33	6562.93	47.25%	117.15%
α=1.00 [%]	0.05%	0.04%	0.04%		
α=1.25 [%]	0.14%	0.10%	0.08%		
Std SHP (150°)	**10 kn**	**11.5kn**	**13kn**	**11.5kn[%]**	**13kn[%]**
α=0.75	55.87	70.99	93.75	27.07%	67.80%
α=1.00	74.44	95.24	125.58	27.94%	68.70%
α=1.25	95.98	120.41	156.43	25.45%	62.98%
α=1.00 [%]	33.24%	34.16%	33.96%		
α=1.25 [%]	71.80%	69.62%	66.87%		

Table 8: Variation of RPM mean value and standard deviation for 150° wave heading and sea state 4.

Mean RPM (150°)	**10 kn**	**11.5kn**	**13kn**	**11.5kn[%]**	**13kn[%]**
α=0.75	63.65	72.60	82.52	14.07%	29.64%
α=1.00	63.65	72.61	82.52	14.07%	29.64%
α=1.25	63.66	72.61	82.52	14.06%	29.63%
α=1.00 [%]	0.00%	0.00%	0.00%		
α=1.25 [%]	0.01%	0.00%	0.00%		
Std RPM (150°)	**10 kn**	**11.5kn**	**13kn**	**11.5kn[%]**	**13kn[%]**
α=0.75	0.71	0.71	0.72	0.73%	1.10%
α=1.00	0.93	0.95	0.95	2.01%	2.13%
α=1.25	1.20	1.20	1.19	-0.51%	-1.38%
α=1.00 [%]	31.99%	33.66%	33.34%		
α=1.25 [%]	70.19%	68.09%	66.02%		

Table 9: Variation of SHP mean value and standard deviation for 150° wave heading and sea state 5.

Mean SHP (150°)	**10 kn**	**11.5kn**	**13kn**	**11.5kn[%]**	**13kn[%]**
α=0.75	4221.63	5800.77	8084.93	37.41%	91.51%
α=1.00	4230.00	5809.43	8094.73	37.34%	91.36%
α=1.25	4241.19	5820.79	8106.85	37.24%	91.15%
α=1.00 [%]	0.20%	0.15%	0.12%		
α=1.25 [%]	0.46%	0.35%	0.27%		
Std SHP (150°)	**10 kn**	**11.5kn**	**13kn**	**11.5kn[%]**	**13kn[%]**
α=0.75	157.09	182.17	220.69	15.97%	40.49%
α=1.00	213.25	245.04	301.79	14.91%	41.52%
α=1.25	269.17	312.80	381.38	16.21%	41.69%
α=1.00 [%]	35.75%	34.51%	36.75%		
α=1.25 [%]	71.35%	71.71%	72.81%		

Table 10: Variation of RPM mean value and standard deviation for 150° wave heading and sea state 5.

Mean RPM (150°)	**10 kn**	**11.5kn**	**13kn**	**11.5kn[%]**	**13kn[%]**
α=0.75	69.46	77.77	87.10	11.97%	25.40%
α=1.00	69.47	77.78	87.11	11.96%	25.39%
α=1.25	69.47	77.79	87.11	11.96%	25.39%
α=1.00 [%]	0.01%	0.00%	0.01%		
α=1.25 [%]	0.02%	0.02%	0.01%		
Std RPM (150°)	**10 kn**	**11.5kn**	**13kn**	**11.5kn[%]**	**13kn[%]**
α=0.75	1.25	1.26	1.25	0.89%	0.44%
α=1.00	1.66	1.67	1.70	0.26%	2.03%
α=1.25	2.09	2.10	2.12	0.57%	1.21%
α=1.00 [%]	33.40%	32.56%	35.51%		
α=1.25 [%]	67.70%	67.17%	68.98%		

It is again observed that the variation of the α-parameter has only marginal impact on the mean values both for power and engine speed, while the range of the percentage change on the STD values for a specific speed in slightly augmented compared to sea-state 4.

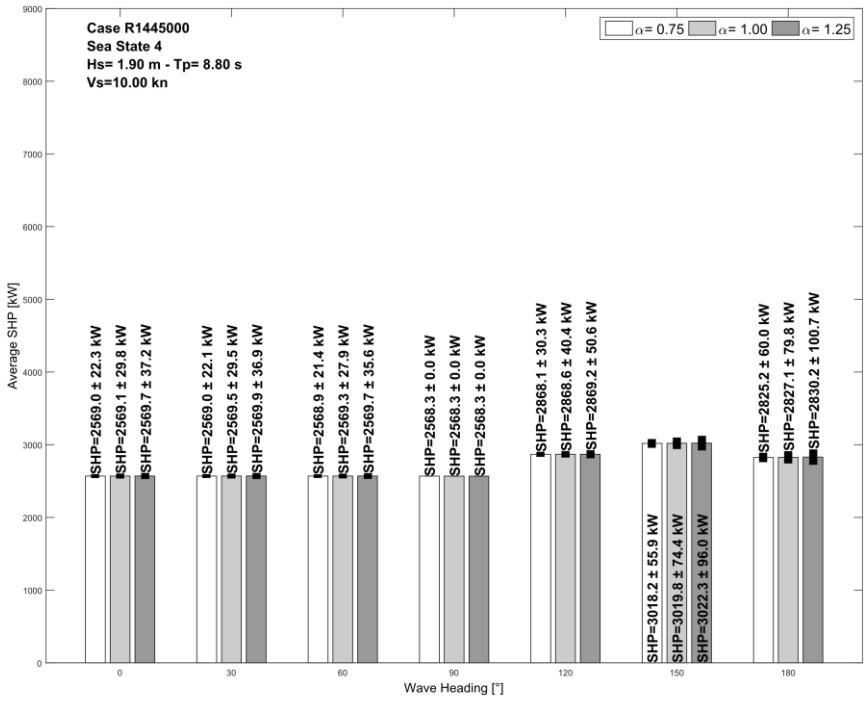

Figure 21: SHP variation for different α. Case 1 - Sea state 4 - Vessel speed 10kn.

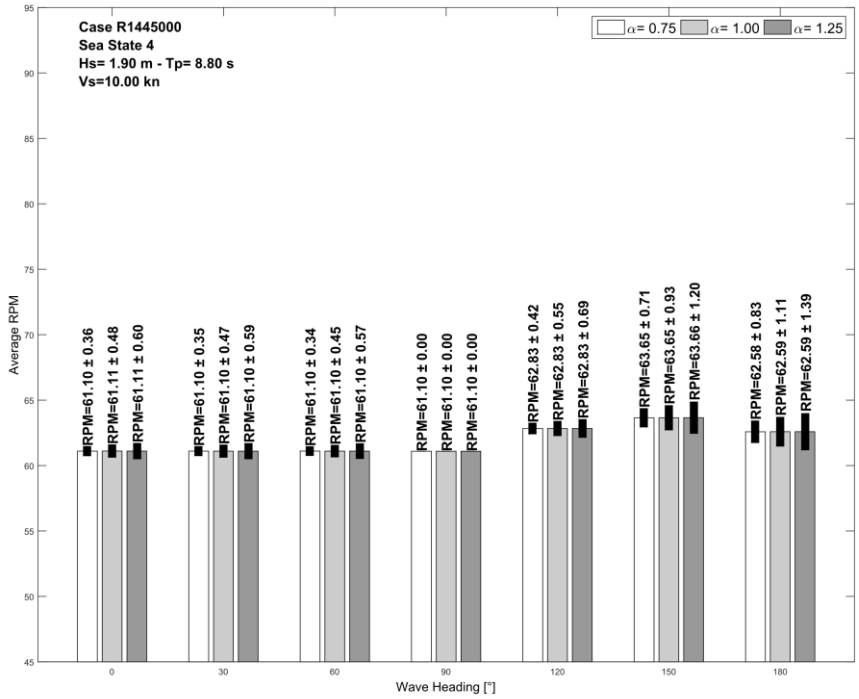

Figure 22: RPM variation for different α. Case 1 - Sea state 4 - Vessel speed 10kn.

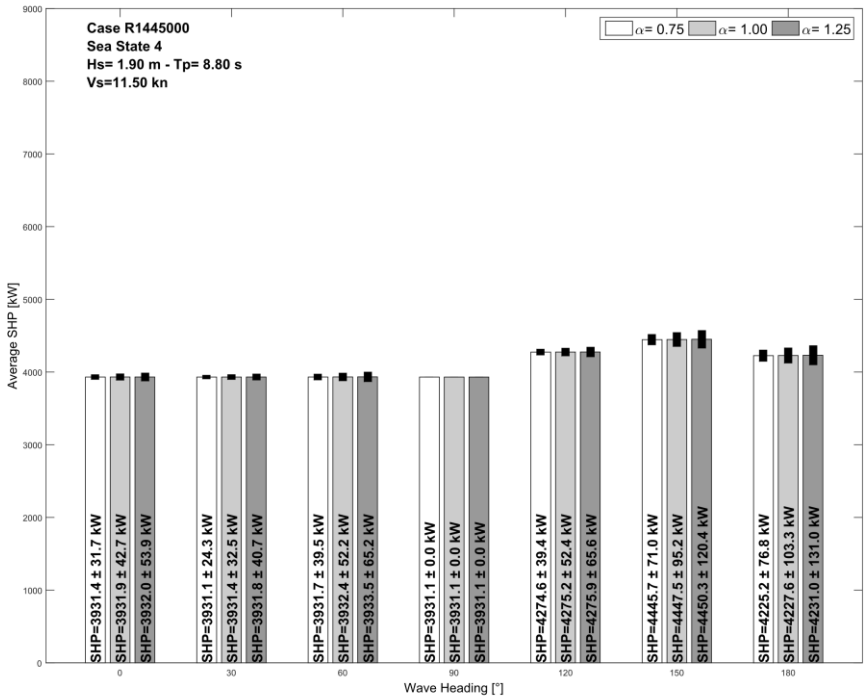

Figure 23: SHP variation for different α. Case 1 - Sea state 4 - Vessel speed 11.5kn.

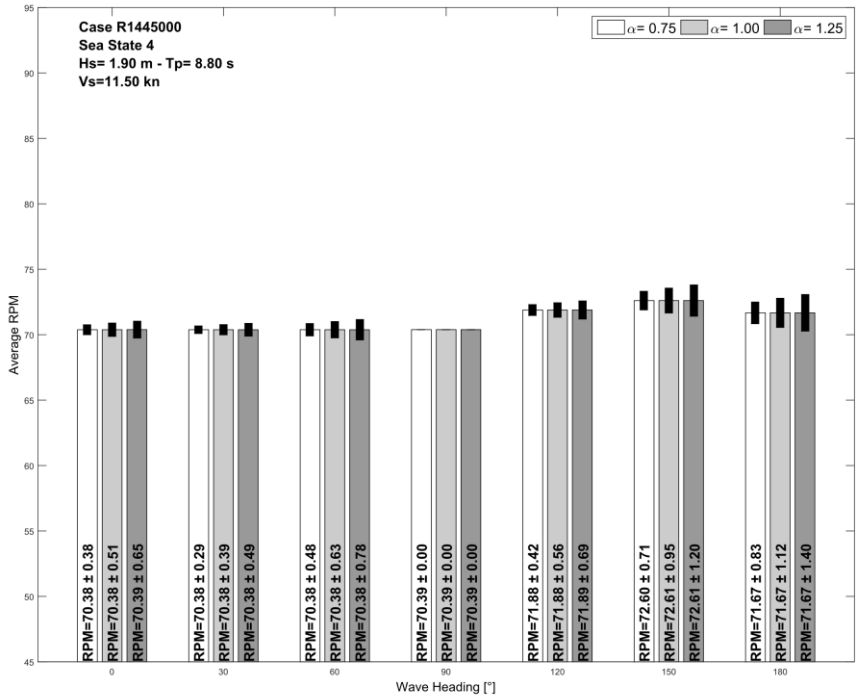

Figure 24: RPM variation for different α. Case 1 - Sea state 4 - Vessel speed 11.5kn.

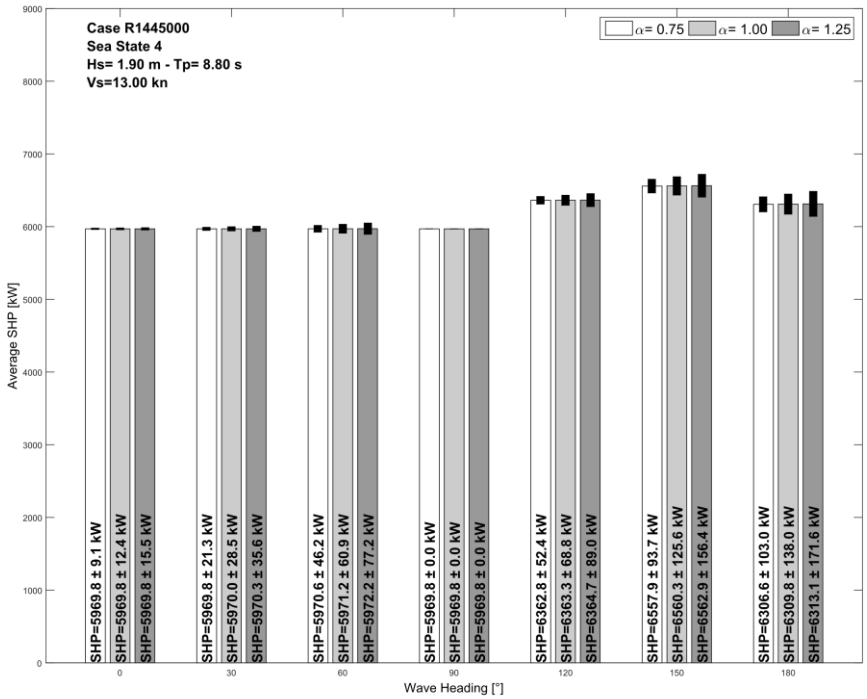

Figure 25: SHP variation for different α. Case 1 - Sea state 4 - Vessel speed 13kn.

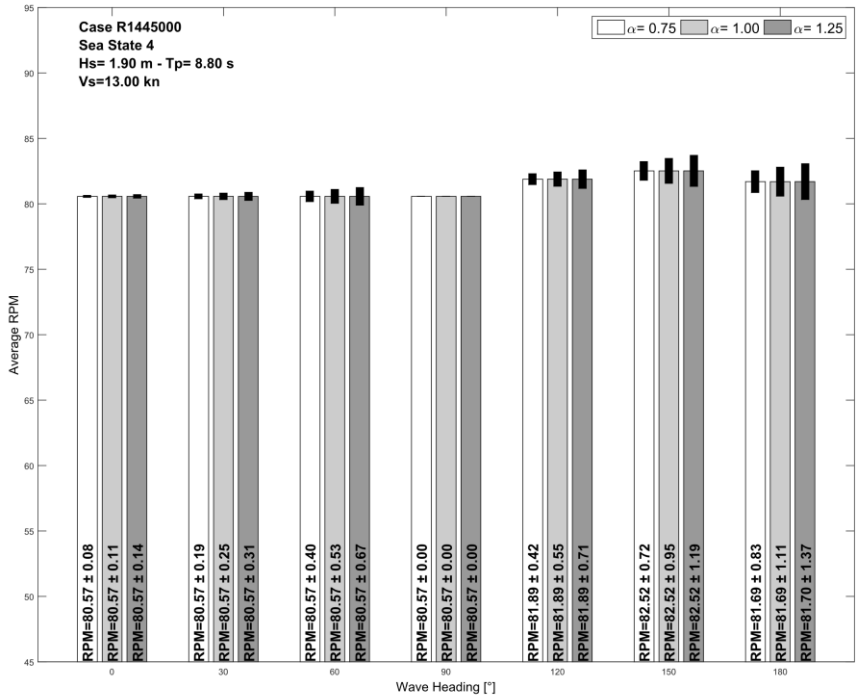

Figure 26: RPM variation for different α. Case 1 - Sea state 4 - Vessel speed 13kn.

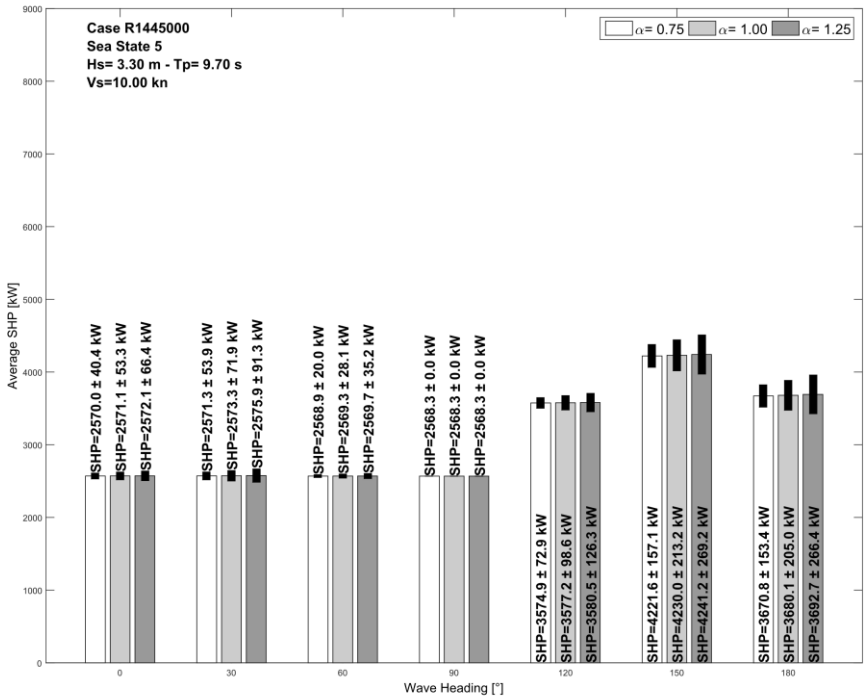

Figure 27: SHP variation for different α. Case 1 - Sea state 5 - Vessel speed 10kn.

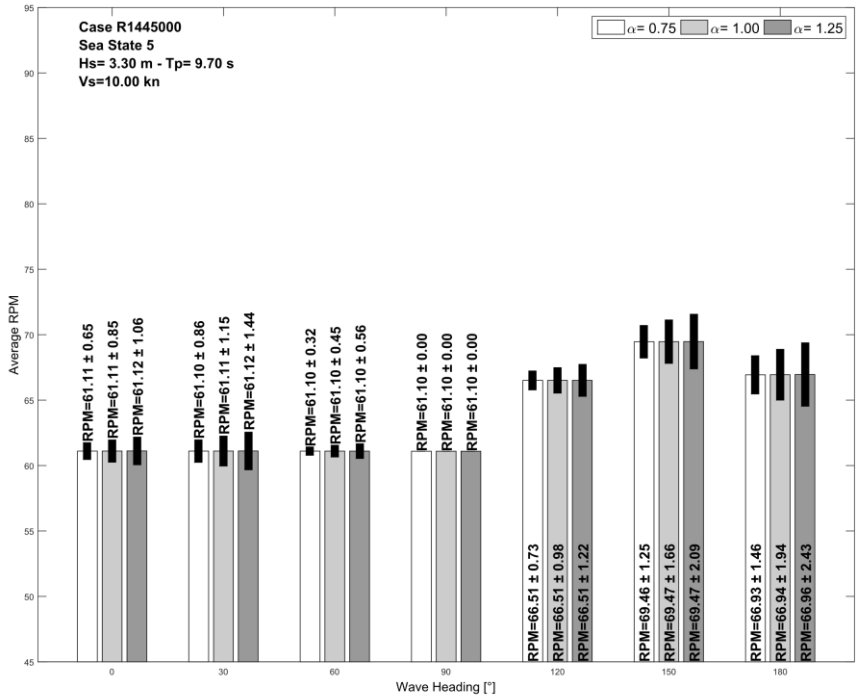

Figure 28: RPM variation for different α. Case 1 - Sea state 5 - Vessel speed 10kn.

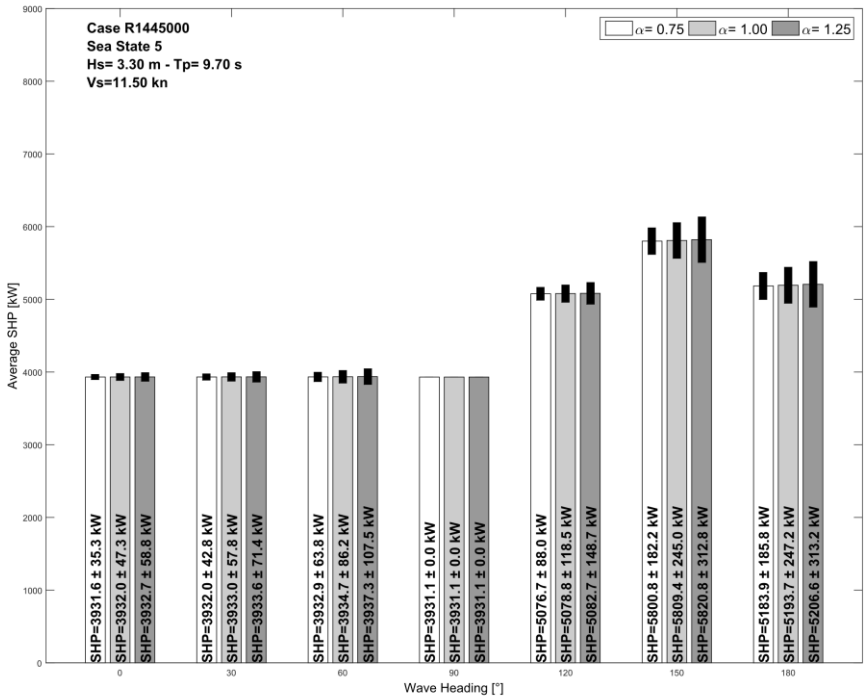

Figure 29: SHP variation for different α. Case 1 - Sea state 5 - Vessel speed 11.5kn.

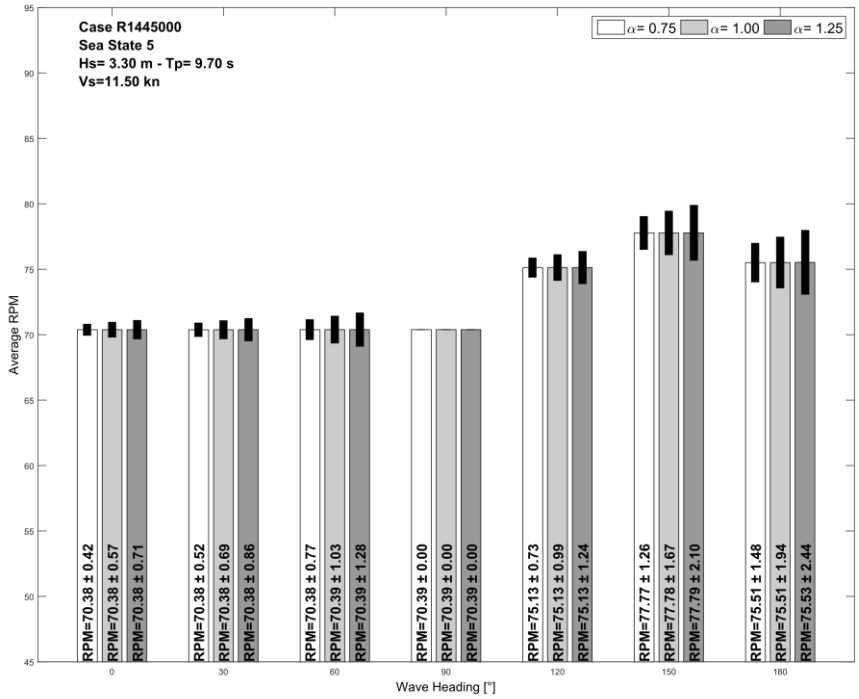

Figure 30: RPM variation for different α. Case 1 - Sea state 5 - Vessel speed 11.5kn.

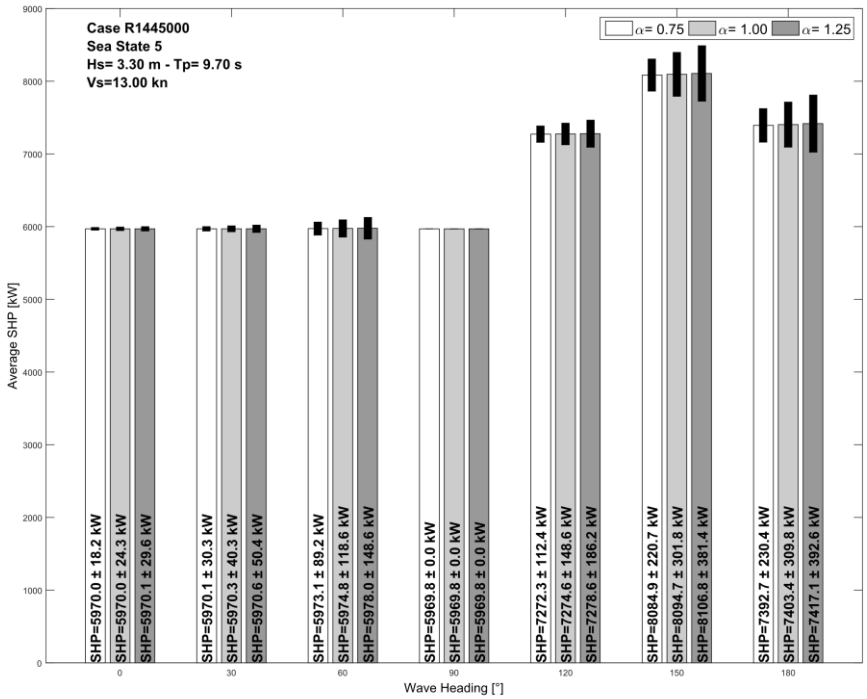

Figure 31: SHP variation for different α. Case 1 - Sea state 5 - Vessel speed 13kn.

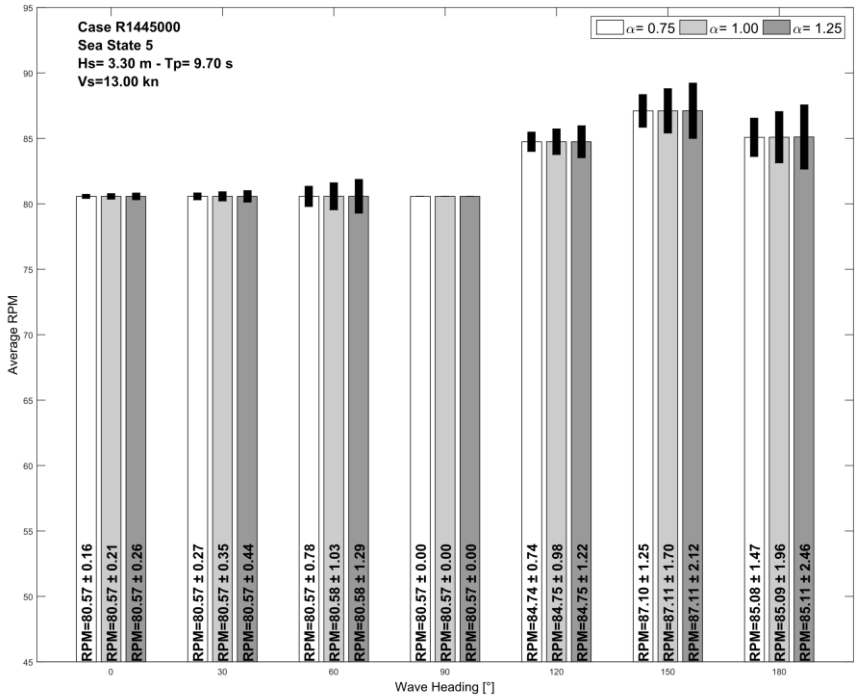

Figure 32: RPM variation for different α. Case 1 - Sea state 5 - Vessel speed 13kn.

5 Conclusions

In the present report a seakeeping model based on strip theory is used to obtain predictions of the mean added wave resistance and ship motion data in waves, which are then used for simulating the system performance, taking into account the effects of wave orbital velocity and the vertical stern motion on the unsteady propeller analysis. The results derived by the present dynamical system, in the case of the studied BC ship, travelling at full draft with speed Vs=14kn in head waves at various sea conditions are presented. The present model facilitates the cost-effective treatment (from the point of view of computational efficiency) of many similar cases required in realistic ship operation, supporting further applications, such as the development of digital-twin systems for optimum weather routing and decision support systems.

In general, it is shown that the parameter-α demonstrates the potential to consider the impact of the wave orbital velocity and the ship's responses in a seaway, as shown by the investigation of the effect of the parameter α in a wide range of environmental conditions and ship speeds. Based on the results obtained on the mean and standard deviation values of the SHP and RPM, it is demonstrated that the α-parameter is effective in capturing the qualitative differences between the examined cases, leading to higher fluctuations on the loading of the engine for more adverse weather conditions and head to bow wave headings. For increasing α-parameter values, a higher standard deviation is obtained, implying more intense fluctuations, while the time-average value of the SHP and RPM remains the same. Furthermore, it was shown that for less sever loading conditions (Case 6) the predicted loading oscillations can have a higher impact on the engine's operational profile, which is due to the operation of the propeller closer to the sea surface, where the wave velocities are more intense.

The developed methodology demonstrates significant potential towards the incorporation of the ship dynamics in the operational performance of the ship. More information and measurements regarding the geometry of the propeller, the wake distribution and the unsteady flow around the propeller would allow the full exploitation of the method to more accurately predict the operational profile of the propulsion system. However, the application of the suggested methodology qualitatively captures the primary effects of the seakeeping response on the operational point of the main engine. Future work includes the comparison and verification of the present simplified model predictions against results obtained by fully-coupled methods based on more sophisticated CFD models for selected conditions, and the calibration of the parameters for the enhancement of its efficiency. Testing in real operational applications of the ship will provide additional information and data for the verification and optimal exploitation of the model. Essentially, the aim of the proposed future work is a more accurate estimation of the α-parameter, which could be achieved by using enhanced predictions of the effective ship wake distribution on the propeller disk and data enabling the modelling of more severe unsteady phenomena that could occur in extreme conditions. In this direction, the incorporation of additional parameters, such as inertia and possible damping effects associated with the drive train could be examined. This can be done by including a model of the shafting-transmission system, covering the most frequent operational profiles of the propulsion system. Finally, the correlation of the present results with on-board measurements requires the acquisition of measurements at a higher frequency (as compared to the standard one in practice today), in conjunction with measurements of the vessel stern motion in waves. This could offer useful data for further research in the subject.

6 References

[1] Papanikolaou, A.D. (2022) "Holistic Approach to Ship Design," *Journal Marine. Science Eng.* 10, 1717. https://doi.org/10.3390/jmse10111717
[2] ITTC 2002, Report of the Resistance Committee, 23rd Inter. Towing Tank Conference.
[3] Spinelli, F., Mancini, S., Vitiello, L., Bilandi, R.N., De Carlini, M. (2022), "Shipping Decarbonization: An Overview of the Different Stern Hydrodynamic Energy Saving Devices," *J. Marine Science and Engineering* 10, 574.
[4] Chou, T., Kosmas, V., Acciaro, M., Renken, K. (2021) "A Comeback of Wind Power in Shipping: An Economic and Operational Review on the Wind-Assisted Ship Propulsion Technology," *Sustainability* 13, 1880.
[5] Muntean T. (2008) "Ship propulsion train efficiency sensing," *Wartsila Technical Journal,* 02.2008.
[6] Belibassakis, K. (2024) "A vortex-element method for the calculation of waves and ship motions effects", Proceedings", The 34th International Ocean and Polar Engineering Conference, Rhodes, Greece.
[7] Nikolaidis, G, Zagkas, V., D'Souza, R., Themelis, N., et al (2024), "D3.1: Hull and propeller performance monitoring tool", Deliverable report for T3.1, RETROFIT55 project.
[8] Belibassakis K., Filippas, E., (2022) "A Dynamical System for the Combined Performance of Innovative Biomimetic Thruster With Standard Propulsion System in Waves," Proc.Int. Conf on *Offshore Mech. and Arctic Engineering* (OMAE2022), Hamburg, Germany.
[9] Belibassakis, K., Politis, G. (2019) "Generation and propagation of noise from cavitating marine propellers," Proc. *6th Intern. Symposium Marine Propulsors* SMP'19, Rome, Italy, May 2019.
[10] Lee, Chang-Sup (1979). Prediction of Steady and Unsteady Performance of Marine Propeller with or without Cavitation by Numerical Lifting Surface Theory, PhD Thesis. Mass. Inst. of Technology.
[11] Belibassakis K.A., Politis, G.K., Gerostathis Th.P. (2013) "Calculation of ship hydrodynamic propulsion in rough seas by non-linear BEM with application to reduction of energy losses in waves," 32nd Int. Conf. on *Offshore Mech. and Arctic Engineering* (OMAE2013), Nantes, France.
[12] Arribas, P.F. (2007) "Some methods to obtain the added resistance of a ship advancing in waves", *Ocean Engineering*, 34, pp. 946–955.
[13] Gerritsma, J., Beukelman, W. (1972) "Analysis of the resistance increase in waves of a fast cargo ship," *International Shipbuilding Progress* 19(217), 285-293.
[14] Loukakis, T.A., Sclavounos, P. (1978) "Some extensions of the classical approach to strip theory of ship motion, including the calculation of mean added forces and moments," *Journal of Ship Research*, 22 (1), pp. 1–19.
[15] Salvesen, N., Tuck, E.O., Faltinsen O., (1970) "Ship motions and sea loads", *Transactions SNAME* 78, pp 250–87.
[16] Lewis, E.V. (Ed), (1989) *Principles of Naval Architecture*, vol. 3, NJ: Society Naval Architects & Marine Engin. (SNAME), New York.
[17] Ochi, M.K. (1998). *Ocean Waves. The Stochastic Approach*, Cambridge University Press.

Appendix A: BC ship data and loading conditions

The principal dimensions and data referring to the examined ship (BC MV Kastor) are listed in Table 11 below from the loading manual:

Table 11: Principal dimensions and data of the examined ship.

Length overall [m]	229.00
Length B.P. at Design Draft [m]	225.50
Breadth moulded [m]	32.26
Depth moulded [m]	20.05
Designed draft moulded [m]	12.20
Scantling draft moulded [m]	14.45
Block coefficient	0.86
Displacement at scantling draft (even keel) [t]	94796.20
Deadweight at scantling draft (even keel) [t]	80996.09
Main Engine	MAN B&W 6S60ME-C8.5-TII X 1set
Service Speed (at designed draft) [kn]	14.30
Complement	25
Gross Tonnage	43933
Net Tonnage	27293
Final Light Ship	
Weight [t]	13800.11
LCG from Aft Peak [m]	98.627
TCG from Centreline [m]	-0.007
VCG above Baseline [m]	11.510

The hull geometry of the ship has been reconstructed using Rhino© and 3D plots illustrating the hull geometrical details are plotted in Figure 33.

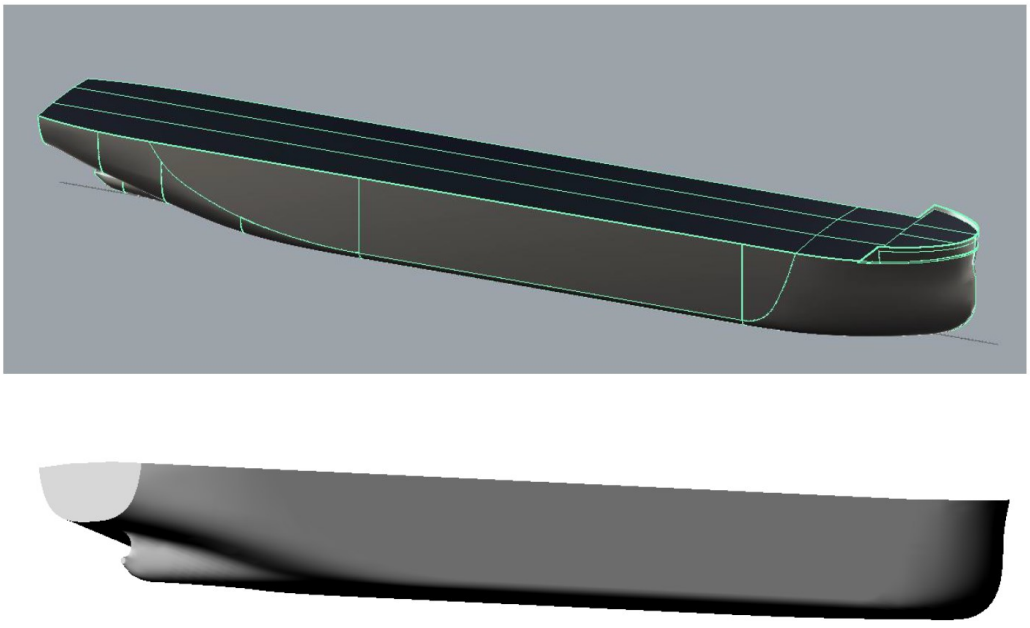

Figure 33: 3D plots of the reconstructed BC ship hull using Rhino©.

In order to proceed with initial hydrostatic and hydrodynamic calculations using NTUA numerical tools, sectional geometry data are extracted at 13 stations of the 3D hull surface, corresponding to the locations of the theoretical sections, as shown in Table 12.

Table 12: Station longitudinal coordinates.

Station	x-coordinate [m] (from transom)	Station	x-coordinate [m] (from transom)	Station	x-coordinate [m] (from transom)
0	0.00	4	91.60	9	206.10
½	11.45	5	114.50	9½	217.55
1	22.90	6	137.40	10	229.00
2	45.80	7	160.30		
3	68.70	8	183.20		

Section geometry is obtained by vertical intersections of the reconstructed 3D hull geometry at the above theoretical locations, and the derived body plan is presented in Figure 34, where also the maximum draft T=14.55m is indicated using a dashed line.

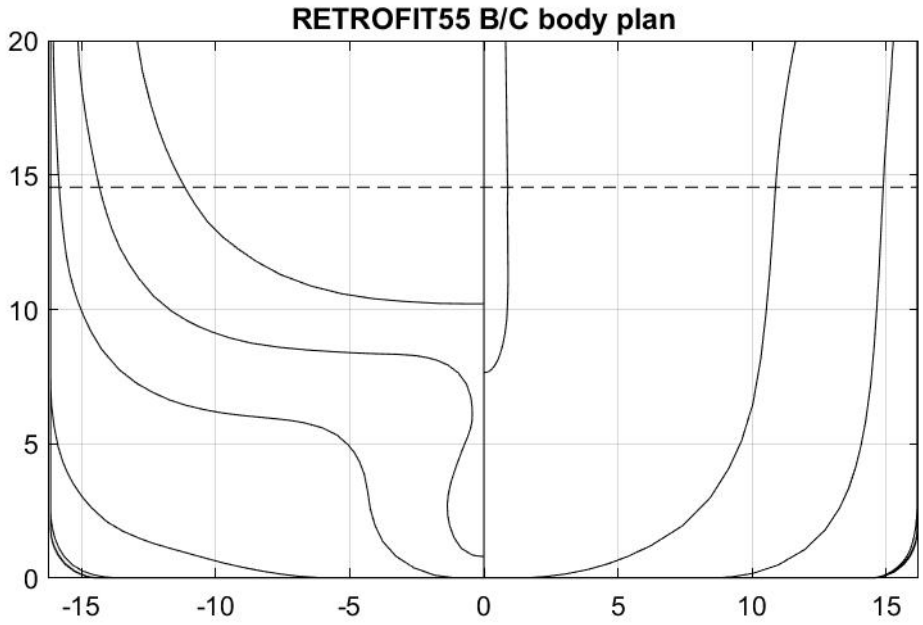

Figure 34: Derived body plan of BC hull from 3D drawing at the 13 theoretical stations. The deck height is set at D=20m from keel.

Also, from operational data the following ship speeds at full loading conditions are identified: Vs=9,11,13,15 kn.

The above data are subsequently used for basic hydrostatic calculations using NTUA tools.

The results of basic hydrostatic calculations for the BC hull are listed in Figure 35.

The calculated results include also data for cross-curves of intact stability for heel angles φ=0°,5°,10°,15°,20°,30°,40° as listed in Figure 36.

```
**********************************************************************************************************
******  RETROFIT55 BULK CARRIER: LBP=229m, B=32.28m, D=20.0m Td=14.45m (3/2023)******
**********************************************************************************************************
CENTER OF GRAVITY IS ASSUMED TO BE AT : XCG = 1.500  YCG = 0.000  ZCG = 0.000
SPECIFIC  GRAVITY OF WATER = 1.025 METRICTONNES/METER 3
SHELL  PLATE  THICKNESS = 0.010 METER
CALCULATIONS ARE PERFORMED FOR  7 ANGLES AND  7 DRAFTS
TRIMMING ANGLE IS 0.0000 (DEG.)
LIST OF UNITS USED FOR THE RESULTS
DISTANCES ,AREAS ETC. : METER
DISPLACEMENT : METRICTONNES
MOMENTS : METRICTONNES*METER

******** HYDROSTATICS ********************************************************
```

DRAFT	AREA	LCF	IMM.VOL.	DISPL.	I TRANS.	I. LONG.	LCB	BM	KB	W.S.	BML
5.00	6131.20	8.239	29027.75	29832.62	490813.4	18937144.0	9.001	16.908	2.581	7723.80	652.40
6.00	6283.90	6.201	35235.29	36200.93	500768.2	20385126.0	8.685	14.212	3.096	8269.20	578.50
6.15	6306.80	5.904	36179.59	37169.68	502934.7	20597950.0	8.617	13.901	3.173	8351.00	569.30
8.00	6478.70	3.843	48052.82	49349.16	525584.8	22180468.0	7.603	10.938	4.138	9270.20	461.60
10.00	6567.10	3.096	61098.63	62730.57	539720.7	23019316.0	6.720	8.834	5.177	10193.40	376.80
12.20	6860.10	-1.258	75861.97	77875.45	555527.8	26287270.0	5.592	7.323	6.331	11408.60	346.50
14.45	**6995.80**	**-3.016**	**92216.27**	**94650.48**	**575332.8**	**27725086.0**	**4.137**	**6.239**	**7.581**	**12566.50**	**300.70**

DRAFT	TP1	MCT1	CB	CWP	CM	CP	CB*	CWP*	CM*	CP*
5.00	3142.23	890.47	0.82288	0.86904	0.98586	0.83468	0.78537	0.82942	0.98586	0.79663
6.00	3220.49	946.51	0.82217	0.87976	0.98822	0.83197	0.79443	0.85008	0.98822	0.80390
6.15	3232.23	954.60	0.82210	0.88135	0.98851	0.83166	0.79583	0.85318	0.98851	0.80508
8.00	3320.34	1007.08	0.82268	0.88734	0.99117	0.83001	0.81257	0.87644	0.99117	0.81981
10.00	3365.64	1033.55	0.82773	0.88967	0.99293	0.83362	0.82654	0.88839	0.99293	0.83242
12.20	3515.78	1178.44	0.84123	0.92807	0.99421	0.84614	0.84119	0.92802	0.99421	0.84609
14.55	**3585.35**	**1242.35**	**0.85717**	**0.94615**	**0.99514**	**0.86135**	**0.85738**	**0.94639**	**0.99514**	**0.86157**

Figure 35: Hydrostatic calculation (extract from NTUA tool) for the reconstructed BC ship hull using offset data of Figure 34.

From Figure 35 we obtain for the max draft T=14.45m the following results (see Table 13) from NTUA hydrostatic calculations:

Table 13: Ship hydrostatics for the maximum draft of 14.45m.

Displacement volume ∇ [m^3]	92216.2
Displacement Δ [t]	94650.0
Long. Pos. of Center of Floatation LCF (aft from midship) [m]	-3.016
Long. Pos. of Center of Buoyancy LCB (forward of midship) [m]	4.137
Vert. Pos. of Center of Buoyancy KB (from keel) [m]	7.581
Trans. Metacentric Radius BM [m]	6.239
Long. Metacentric Radius BM_L [m]	300.7
Waterplane area A_{WP} [m^2]	6995.8
Wetted surface area W.S. (without appendages) [m^2]	12566.5
Block coefficient c_B	0.857
Prismatic coefficient c_p	0.861
Midship section coefficient c_M	0.995
Waterplane area coefficient c_{WP}	0.946

Comparing the calculated displacement Δ=94650ton with the one reported in the ship manual Δ=94796t we consider the above approximation to be very good for proceeding with hydrodynamic

calculations. Using the above, the cross-curve data are calculated for the reconstructed BC hull. The latter, in conjunction with the position of the vertical center of gravity allow intact stability calculations.

As an example, assuming KG at 0.55*D from keel, i.e. KG=11m for the BC at the full loading condition for draft T=14.55m which is quite compatible with the data from the ship loading manual (for example for the LOAD22: Homogeneous Light Cargo (0.819 t/m3), VCG=11.2m) the metacentric height is calculated to be: GM=KB+BM-KG= 7.58+6.24-11=2.82m and the stability diagram is presented in Figure 10.

ANGLE OF HEEL IS 0.000 DEG.

IMM.VOL.	DISPLAC.	RIG.ARM.	RIG.MOM.	Y.C.B.	Z.C.B.
29027.8	29832.6	0.000	0.0	0.00	2.58
35235.3	36200.9	0.000	0.0	0.00	3.10
36179.6	37169.7	0.000	0.0	0.00	3.17
48052.8	49349.2	0.000	0.0	0.00	4.14
61098.6	62730.6	0.000	0.0	0.00	5.18
75862.0	77875.5	0.000	0.0	0.00	6.33
92216.3	94650.5	0.000	0.0	0.00	7.58

ANGLE OF HEEL IS 5.000 DEG.

IMM.VOL.	DISPLAC.	RIG.ARM.	RIG.MOM.	Y.C.B.	Z.C.B.
29057.9	29863.9	1.701	50798.4	1.48	2.65
35311.5	36279.4	1.515	54963.3	1.25	3.16
36180.4	37170.7	1.497	55644.6	1.22	3.23
48197.3	49497.4	1.316	65138.5	0.95	4.19
61184.4	62818.6	1.221	76701.5	0.77	5.22
76234.7	78257.9	1.194	93440.0	0.64	6.39
92376.8	94815.2	1.206	114347.1	0.54	7.62

ANGLE OF HEEL IS 10.000 DEG.

IMM.VOL.	DISPLAC.	RIG.ARM.	RIG.MOM.	Y.C.B.	Z.C.B.
29402.2	30217.8	3.401	102770.9	2.95	2.87
35264.6	36231.3	3.055	110686.5	2.52	3.32
36180.5	37170.8	3.013	111995.5	2.46	3.39
48196.1	49495.9	2.640	130669.3	1.92	4.32
61223.9	62859.4	2.448	153879.9	1.55	5.32
76227.7	78250.6	2.395	187410.2	1.29	6.47
91227.5	93651.1	2.246	210340.5	0.94	7.58

ANGLE OF HEEL IS 15.000 DEG.

IMM.VOL.	DISPLAC.	RIG.ARM.	RIG.MOM.	Y.C.B.	Z.C.B.
29792.8	30618.6	5.099	156124	4.41	3.23
35287.4	36254.8	4.620	167497.2	3.82	3.61
36180.4	37170.8	4.557	169387.4	3.73	3.67
48182.1	49481.5	3.982	197035.2	2.91	4.54
61303.9	62942.4	3.698	232761.2	2.35	5.51
75992.4	78011.9	3.588	279906.7	1.95	6.60
89823.6	92216.5	3.138	289375.5	1.23	7.53

ANGLE OF HEEL IS 20.000 DEG.

IMM.VOL.	DISPLAC.	RIG.ARM.	RIG.MOM.	Y.C.B.	Z.C.B.
30354.7	31193.7	6.687	208592.0	5.76	3.72
35369.3	36338.7	6.189	224900.0	5.12	4.03
36181.4	37171.8	6.118	227417.1	5.03	4.08
48306.0	49608.5	5.349	265355.8	3.92	4.87
61425.9	63068.0	4.976	313826.3	3.19	5.78
74938.1	76936.0	4.628	356059.6	2.49	6.68
89534.9	91924.6	3.892	357770.5	1.39	7.56

ANGLE OF HEEL IS 30.000 DEG.

IMM.VOL.	DISPLAC.	RIG.ARM.	RIG.MOM.	Y.C.B.	Z.C.B.
34067.8	34998.7	8.845	309563.3	7.38	4.91
35244.8	36206.6	8.777	317785.4	7.25	5.00
36185.5	37171.9	8.724	324288.1	7.15	5.06
48743.0	50059.2	8.057	403327.1	5.93	5.84
60937.2	62573.8	7.209	451094.7	4.63	6.40
74651.9	76649.0	6.228	477370.2	3.17	6.97
89521.1	91915.2	5.178	475936.9	1.57	7.64

ANGLE OF HEEL IS 40.000 DEG.

IMM.VOL.	DISPLAC.	RIG.ARM.	RIG.MOM.	Y.C.B.	Z.C.B.
29048.5	29846.1	10.710	319651.4	9.34	5.53
35284.0	36246.2	10.459	379098.8	8.65	5.97
36179.6	37165.4	10.413	387003.0	8.54	6.02
48080.8	49381.0	9.652	476625.7	7.09	6.56
60966.8	62607.0	8.628	540173.5	5.43	6.95
75386.6	77406.4	7.364	570020.8	3.50	7.28
89782.2	92185.4	6.235	574775.8	1.66	7.73

Figure 36: Cross-curve data for the examined ship using offset data of Figure 34.

Based on the above hydrodynamic seakeeping calculations are obtained for the BC ship in head waves (β=180°), quartering seas (β=150°), nearly beam seas (β=120°), and a set of vessel speeds Vs=9,11,13,15kn. The selected conditions from the ship loading manual, which are examined, are listed in Table 14.

Table 14: Selected conditions examined for the examined ship from the ship loading manual.

name of condition	filename		draufts					wave characteristics		
			Tm	T_F	T_A	Trim**	Ship Speed	Hs	Tp	mean direction*
			m	*m*	*m*	*m*	*kn*	*m*	*s*	*deg*
Homogenous Light Cargo (0.804t/m^3) departure	1	R1445000	14.45	14.45	14.45	0	9		7.5	180
							11	2.5	9	150
							13	5	11	120
							15		13	80
									15	
	2	R1445050		14.2	14.7	-0.5	9		7.5	180
							11	2.5	9	150
							13	5	11	120
							15		13	80
									15	
Normal Ballast at Departure	3	R0635320	6.35	4.75	7.95	-3.2	10		7.5	180
							12	2.5	9	150
							14	5	11	120
							16		13	80
									15	
	4	R0635275		4.975	7.725	-2.75	10		7.5	180
							12	2.5	9	150
							14	5	11	120
							16		13	80
									15	
Laden condition derived from operational data	5	R1300000	13	13	13	0			7.5	180
							11	2.5	9	150
							13	5	11	120
							15		13	80
									15	
	6	R1300050		13.25	12.75	-0.5			7.5	180
							11	2.5	9	150
							13	5	11	120
							15		13	80
									15	
Heavy Ballast at midway	7	R0825225	8.25			-2.25	9	2	7.5	180
							11	2.5	9	150
							13	5	11	120
							15		13	80
									15	

In particular, for the BC at T=14.55m corresponding to the full loading conditions without trim, the following estimations (see Table 14) are used in the calculations:

Table 15: Estimated ship inertial characteristics.

Vert. Pos. of Center of Gravity KG [m] (from keel)	11.00
Long. Pos. of Center of Gravity LCG (=LCB) [m]	4.13
Trans. Metacentric height GM [m]	2.82
Radius of Gyration in roll R_{xx} (25% of beam) [m]	8.00
Radius of Gyration in pitch R_{yy} (15% of length) [m]	34.30

Seakeeping calculations are based on Frank close-fit method (see, e.g. [16]) implementing strip theory as proposed by [15] on the two-dimensional results derived for the ship sections.

The various selected cases examined representing more frequent loading conditions of the BC ship are listed in Table 14. As an example, the cases of Homogenous Light Cargo (0.804t/m3) departure, and (b) Normal Ballast Condition (departure) are indicated in Figure 37. For all examined cases, different ship hull sectional data are derived for the various selected conditions of Table 14 in order to account for trim effects, as presented in Figure 38.

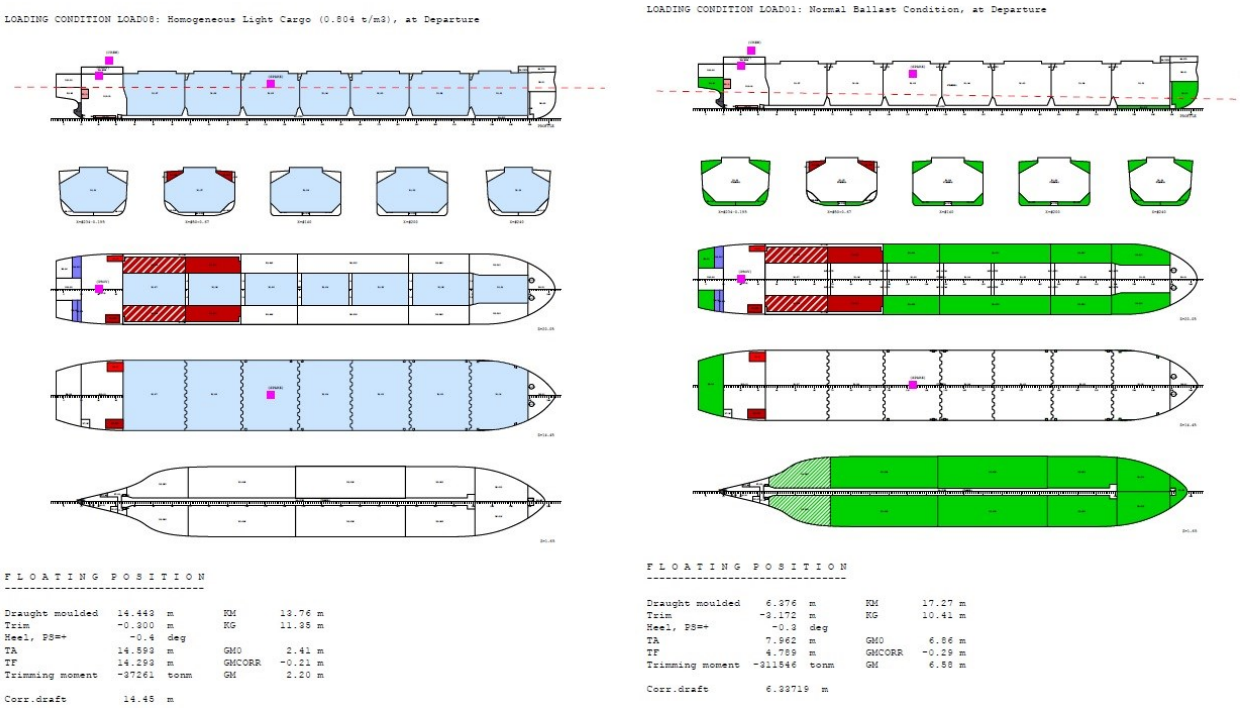

Figure 37: Indicative loading conditions. (Left) Homogenous Light Cargo (0.804t/m3) departure, and (Right) Normal Ballast Condition (departure).

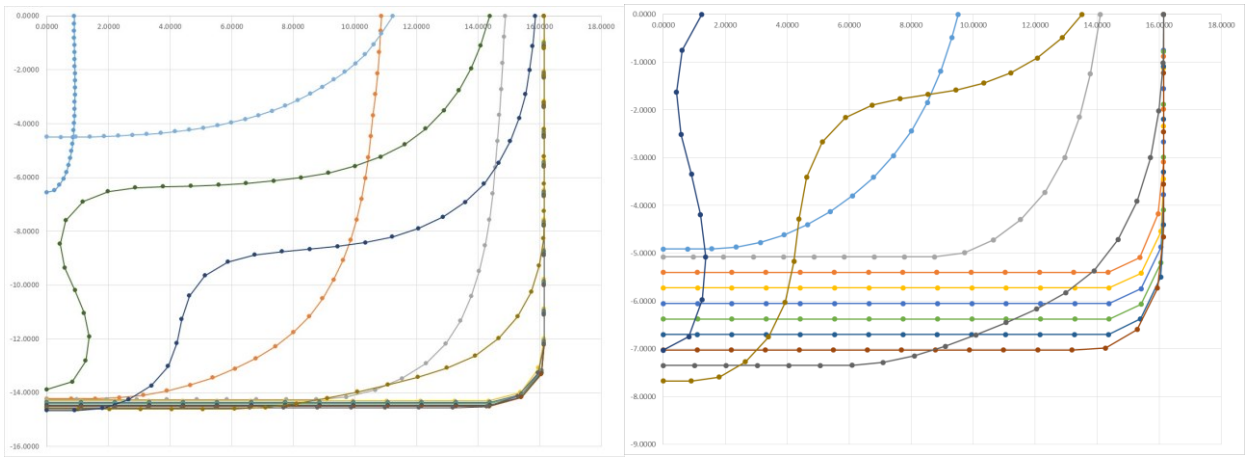

Figure 38: Approximation of sectional curves (left) in full load condition with very small trim and (right) in ballast condition with trim.

The Frank code forms an alternative calculations methodology to SPP-86. It accepts as input the coordinates of the points lying on the contour of each cross section of a ship hull and calculates the respective two-dimensional complex potential for each one of the heave, sway and roll motions, by defining the strengths of the sources distributed across the section's contour. Then, by integrating in the longitudinal direction, it calculates the hydrodynamic factors of added mass and damping, for the given frequency.

The software calculates also the added resistance of ships in irregular waves characterised by frequency spectrum at various incident wave directions using the energy method of [14].

For the calculated mean added wave resistance, an extrapolation method is used to obtain results in intermediate conditions and for operation in following seas. For ship speeds outside the interval from Vs= 9kn to Vs=14kn, as well as for significant wave height outside the interval from Hs=2.5m to 5m and for peak periods outside the interval from Tp=7.5 to 15sec, appropriate extrapolation scheme is used. A Matlab© function is developed and provided for the prediction of the BC ship performance in waves using the dynamical system described in this report.

Appendix B: BC ship seakeeping results

Indicative tabular information and data obtained by seakeeping analysis of the BC ship are shown in Figure 39 concerning various responses. The detailed data for all loading conditions considered and various ship speeds and wave conditions as calculated by the Frank method is provided in xls-file form. Additional data regarding the mean added wave resistance are also provided in similar form, for all examined combinations. Indicative results are presented in Figure 40.

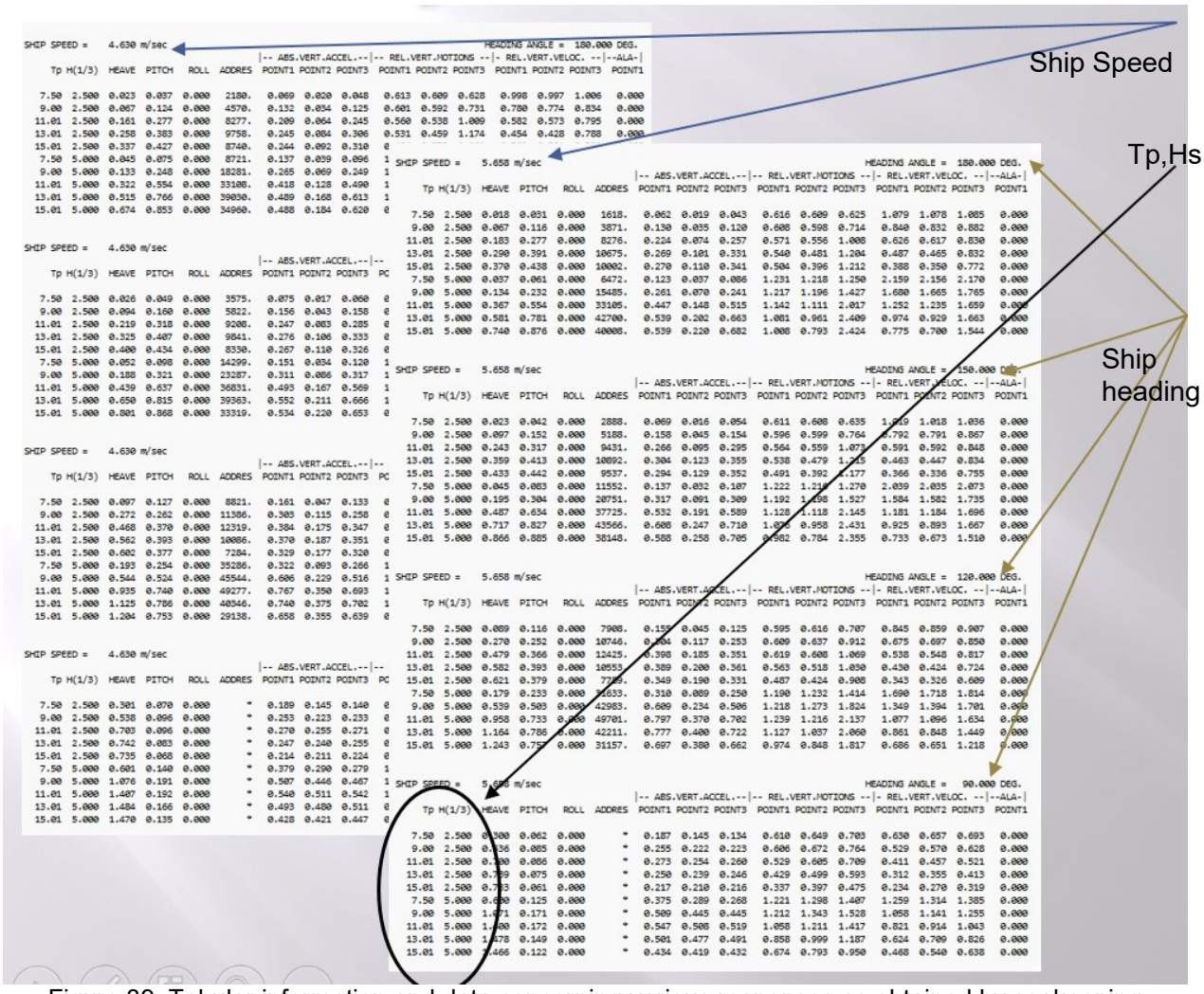

Figure 39: Tabular information and data concerning various responses as obtained by seakeeping analysis of the examined ship.

Calculated results concerning the mean added wave resistance for all loading conditions considered for the examined ship, for various ship speed and wave conditions are shown in Figure 41-Figure 46, respectively. Finally, a comparison of the results for several loading conditions of the examined ship for speed Vs=11-12kn and head waves of Hs=2.5m and various peak periods is presented in Figure 47.

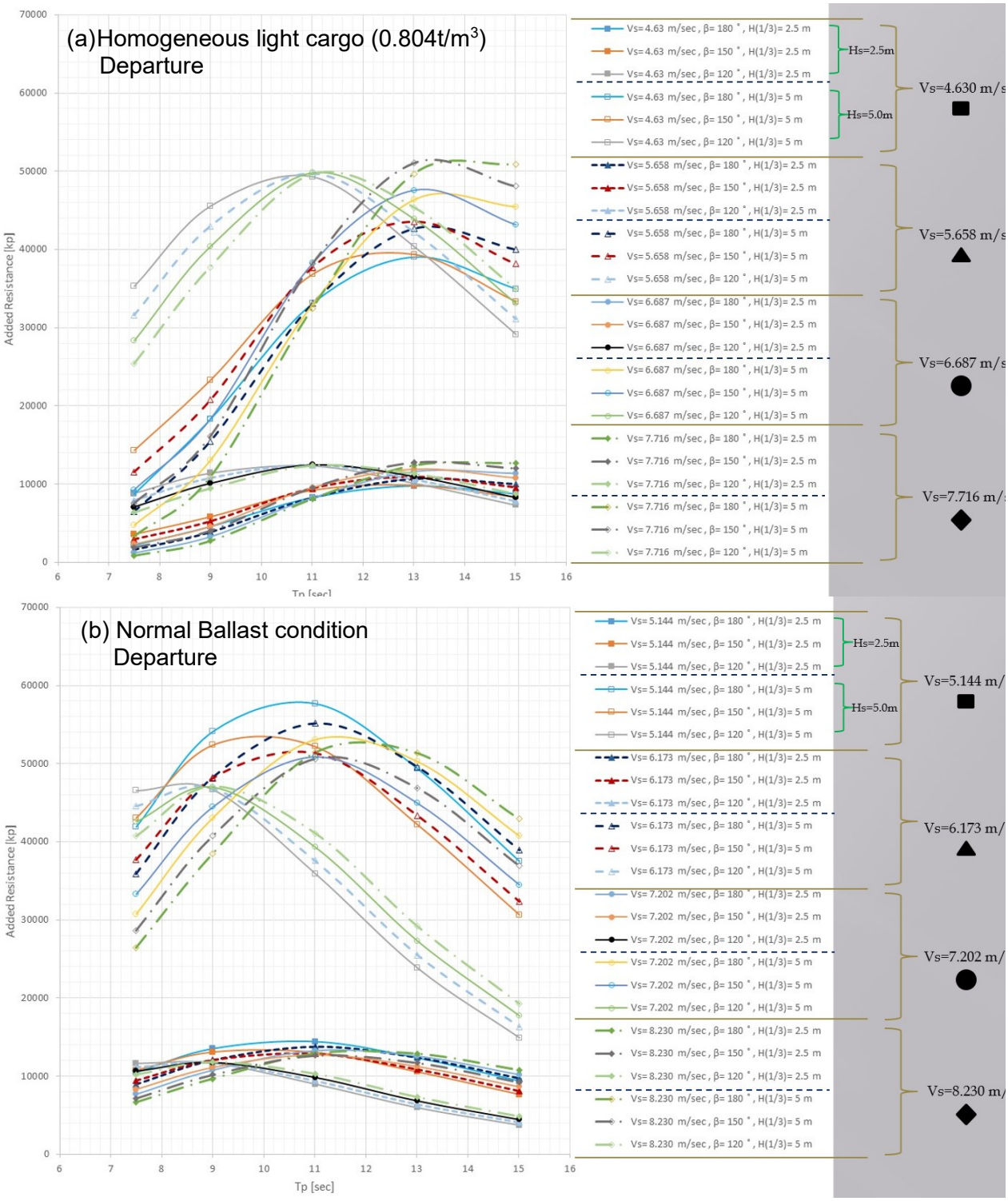

Figure 40: Calculated results of the mean added wave resistance as obtained by seakeeping analysis of the examined ship, for various ship speeds and wave conditions and for loading conditions (a) Homogeneous light cargo – Departure and (b) Normal Ballast condition – Departure.

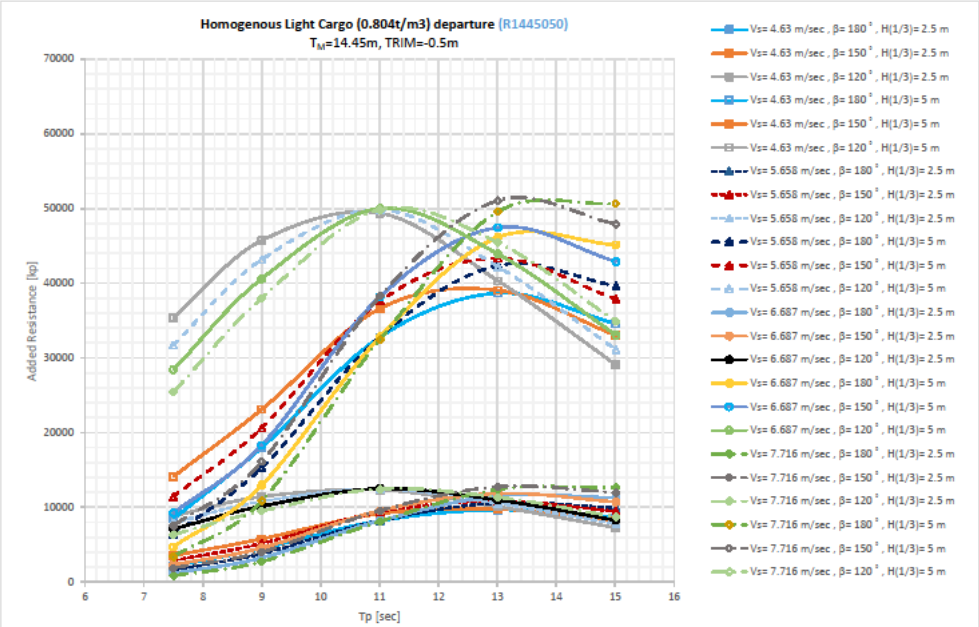

Figure 41: Calculated results of the mean added wave resistance for loading condition R1445050 for various ship speed and wave conditions.

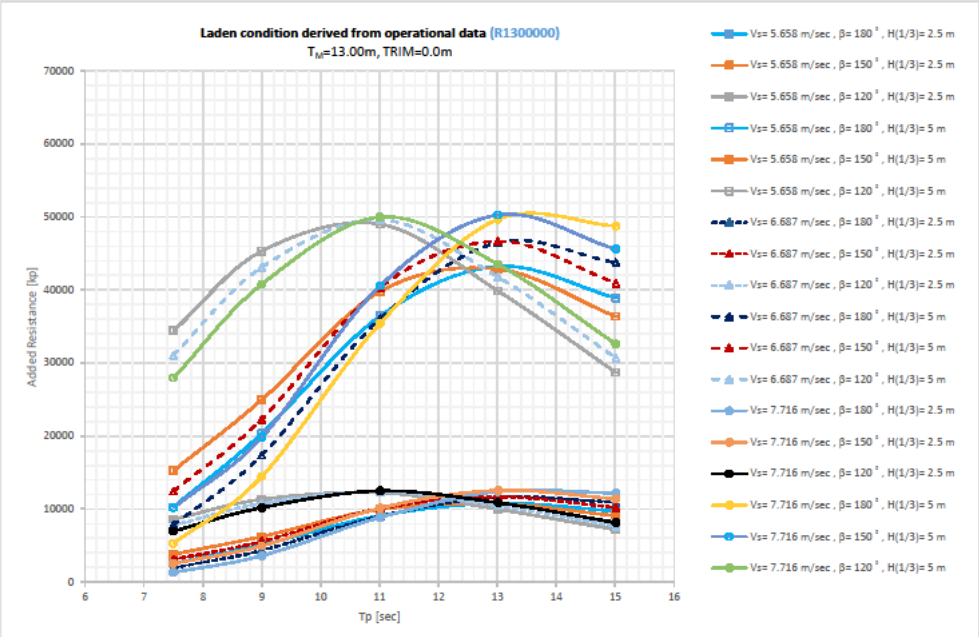

Figure 42: Calculated results of the mean added wave resistance for loading condition R1300000 for various ship speed and wave conditions.

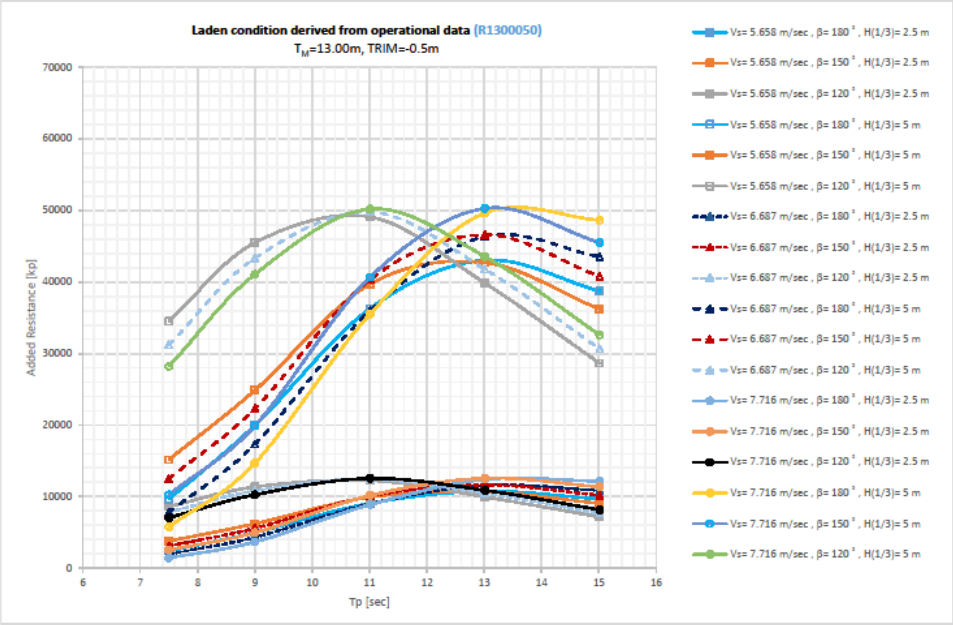

Figure 43: Calculated results of the mean added wave resistance for loading condition R1330050 for various ship speed and wave conditions.

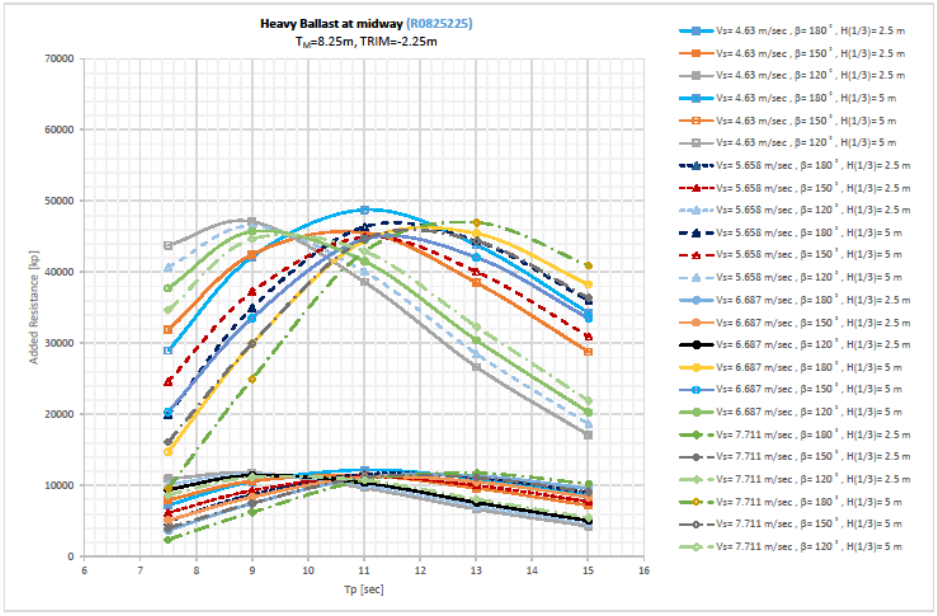

Figure 44: Calculated results of the mean added wave resistance for loading condition R0825225 for various ship speed and wave conditions.

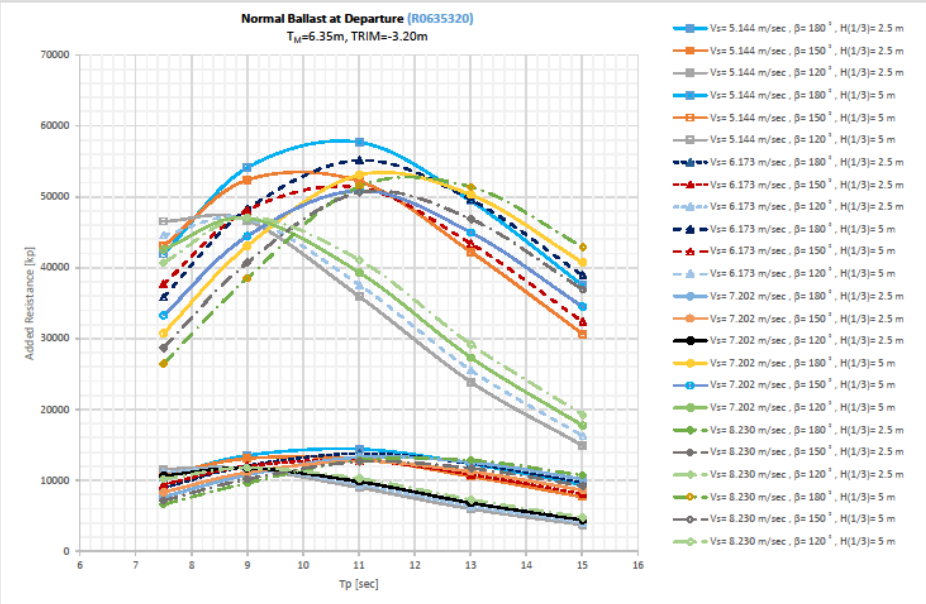

Figure 45: Calculated results of the mean added wave resistance for loading condition R0635320 for various ship speed and wave conditions.

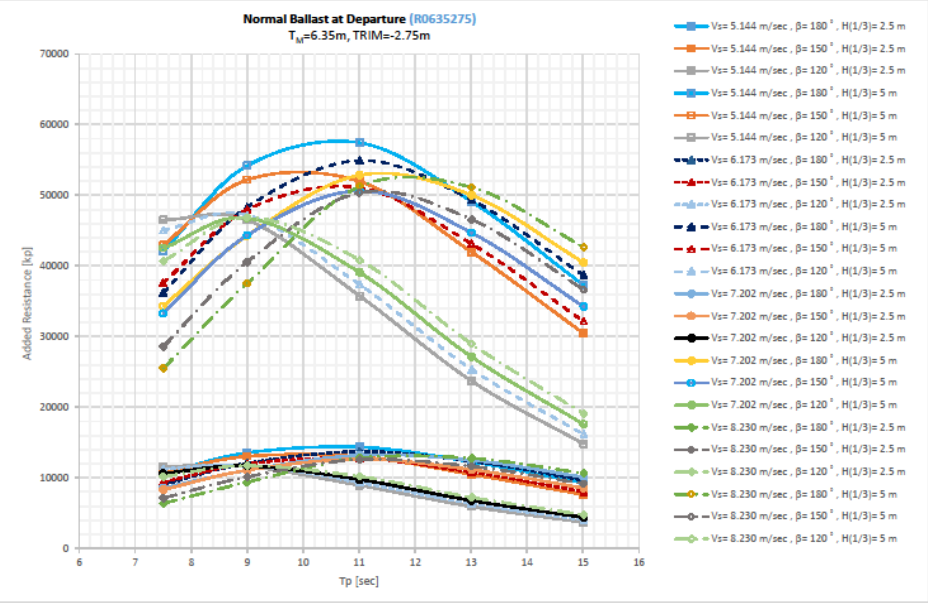

Figure 46: Calculated results of the mean added wave resistance for loading condition R0635275 for various ship speed and wave conditions.

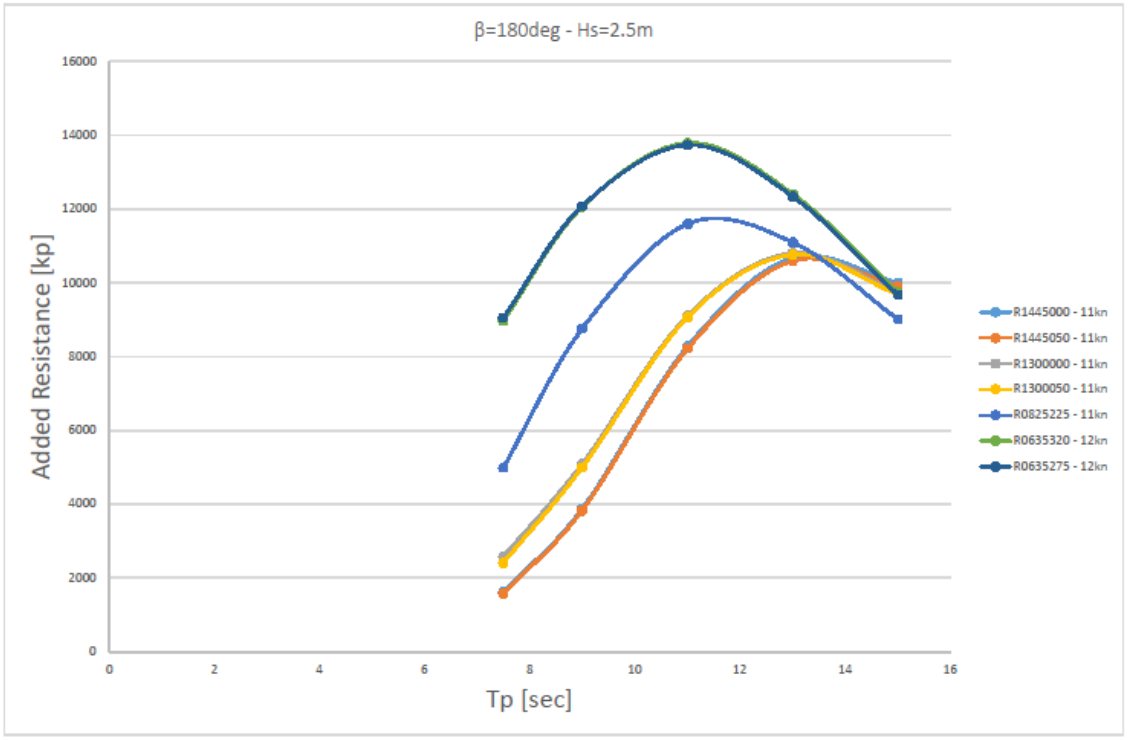

Figure 47: Comparison of results concerning the mean added wave resistance for several loading conditions of the examined ship for speed Vs=11-12kn and head waves of Hs=2.5m and various peak periods.

Appendix C: Loading condition R1300050 (Case 6) α-parameter effect

In this Appendix the results obtained regarding the parametric analysis of the α-parameter, with reference to Loading condition R1300050 (Case 6), are discussed. The results are presented in Figure 48-Figure 59, with the colors representing one value of the α-parameter and the plots organized as discussed in section 4.4, while Table 16-Table 19 summarize the results obtained for 150° wave direction, which represents the worst case scenario in terms of power consumption. To begin with the comparison against the results obtained for R1445000 (Case 1), it can be observed that a reduction on the average SHP requirement and engine speed is predicted, for the same environmental conditions and ship speed. This is attributed to the lower draft (by about 1.5m) and the respective calm water resistance component reduction.

Qualitatively the general trend of the α-parameter effect is demonstrated also in this case. To be more specific, it can be observed that the mean value of SHP and RPM remain almost constant over the range of examined α values, for the same ship speed, wave direction and sea state. Regarding the standard deviation variation with different α values, it can be observed that the trend leading to higher standard deviation values for increasing α values is generally confirmed also for this loading condition. It has to be noted however, that the standard deviation value for the herein examined loading condition is more sensitive to the change of the α-parameter, for the same vessel speed, wave direction and sea state, compared to case 1. For example, for Vs=10kn and sea state 5, in the 150° wave direction the percentage change of the SHP standard deviation is 36% for α=1 and 71% for α=1.25 in Case 1, while in Case 6 the corresponding change is 41% and 110%. Another observation is that for example in sea state 5 and 13 knots forward vessel speed the standard deviation of SHP for Case 6 is approximately 20-30 kW less than the SHP standard deviation for Case 1, while the mean SHP value is 4850kW for Case 6 and 8100kW for Case 1. Therefore, the standard deviation in case 6 corresponds to a higher fraction of the mean SHP value, which is also graphically illustrated in the following figures by the ratio of the black slender bar heights against the column heights. This behavior is attributed to the lower draft, compared to Case 1, because the propeller is closer to the sea surface. Consequently the wave orbital velocities corresponding to the depth of the propeller, are less diminished and they have a higher impact on the standard deviation of the results, which is further amplified by increasing the α-parameter. As a result, it is anticipated that for lower drafts the impact of the wave orbital velocities and the seakeeping performance of the vessel is more significant and thus it can cause more intensive loading fluctuations on the engine.

Table 16: Variation of SHP mean value and standard deviation for 150° wave heading and sea state 4.

Mean SHP (150°)	**10 kn**	**11.5kn**	**13kn**	**11.5kn[%]**	**13kn[%]**
α=0.75	1670.05	2399.15	3460.13	43.66%	107.19%
α=1.00	1673.19	2402.58	3464.49	43.59%	107.06%
α=1.25	1677.75	2407.38	3469.41	43.49%	106.79%
α=1.00 [%]	0.19%	0.14%	0.13%		
α=1.25 [%]	0.46%	0.34%	0.27%		
Std SHP (150°)	**10 kn**	**11.5kn**	**13kn**	**11.5kn[%]**	**13kn[%]**
α=0.75	46.82	56.61	71.07	20.91%	51.80%
α=1.00	63.42	76.97	98.42	21.37%	55.19%
α=1.25	83.12	98.31	125.50	18.28%	50.98%
α=1.00 [%]	35.46%	35.98%	38.49%		
α=1.25 [%]	77.55%	73.68%	76.59%		

Table 17: Variation of RPM mean value and standard deviation for 150° wave heading and sea state 4.

Mean RPM (150°)	10 kn	11.5kn	13kn	11.5kn[%]	13kn[%]
α=0.75	54.99	62.41	70.53	13.49%	28.25%
α=1.00	55.01	62.43	70.53	13.48%	28.22%
α=1.25	55.02	62.43	70.55	13.47%	28.21%
α=1.00 [%]	0.03%	0.02%	0.01%		
α=1.25 [%]	0.05%	0.04%	0.03%		
Std RPM (150°)	**10 kn**	**11.5kn**	**13kn**	**11.5kn[%]**	**13kn[%]**
α=0.75	1.45	1.46	1.46	0.86%	0.82%
α=1.00	1.94	1.98	1.98	1.97%	2.15%
α=1.25	2.46	2.49	2.45	1.02%	-0.26%
α=1.00 [%]	34.04%	35.51%	35.81%		
α=1.25 [%]	69.97%	70.23%	68.15%		

Table 18: Variation of SHP mean value and standard deviation for 150° wave heading and sea state 5.

Mean SHP (150°)	10 kn	11.5kn	13kn	11.5kn[%]	13kn[%]
α=0.75	2759.87	3611.56	4812.39	30.86%	74.37%
α=1.00	2777.58	3628.37	4827.27	30.63%	73.79%
α=1.25	2804.15	3649.82	4849.77	30.16%	72.95%
α=1.00 [%]	0.64%	0.47%	0.31%		
α=1.25 [%]	1.60%	1.06%	0.78%		
Std SHP (150°)	**10 kn**	**11.5kn**	**13kn**	**11.5kn[%]**	**13kn[%]**
α=0.75	164.16	175.80	200.48	7.09%	22.13%
α=1.00	231.17	245.56	272.80	6.22%	18.01%
α=1.25	345.10	325.10	351.35	-5.79%	1.81%
α=1.00 [%]	40.82%	39.68%	36.08%		
α=1.25 [%]	110.23%	84.93%	75.26%		

Table 19: Variation of RPM mean value and standard deviation for 150° wave heading and sea state 5.

Mean RPM (150°)	10 kn	11.5kn	13kn	11.5kn[%]	13kn[%]
α=0.75	62.14	68.84	76.29	10.78%	22.76%
α=1.00	62.17	68.86	76.32	10.77%	22.78%
α=1.25	62.20	68.90	76.34	10.76%	22.73%
α=1.00 [%]	0.03%	0.03%	0.05%		
α=1.25 [%]	0.10%	0.09%	0.07%		
Std RPM (150°)	**10 kn**	**11.5kn**	**13kn**	**11.5kn[%]**	**13kn[%]**
α=0.75	2.29	2.32	2.34	1.36%	2.37%
α=1.00	3.08	3.14	3.12	1.93%	1.45%
α=1.25	3.82	3.89	3.93	1.74%	2.75%
α=1.00 [%]	34.56%	35.31%	33.35%		
α=1.25 [%]	67.08%	67.71%	67.71%		

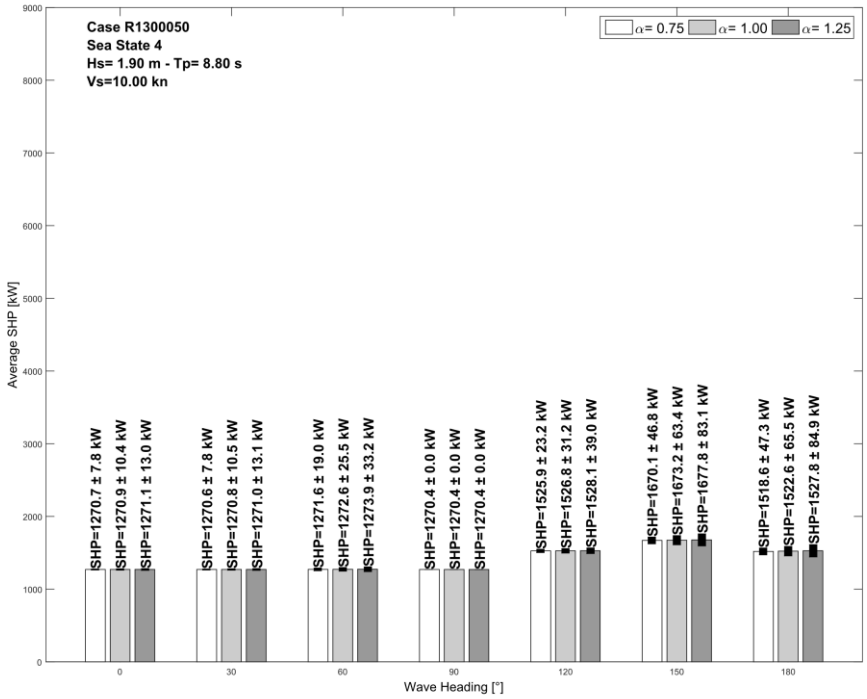

Figure 48: SHP variation for different α. Case 6 - Sea state 4 - Vessel speed 10kn.

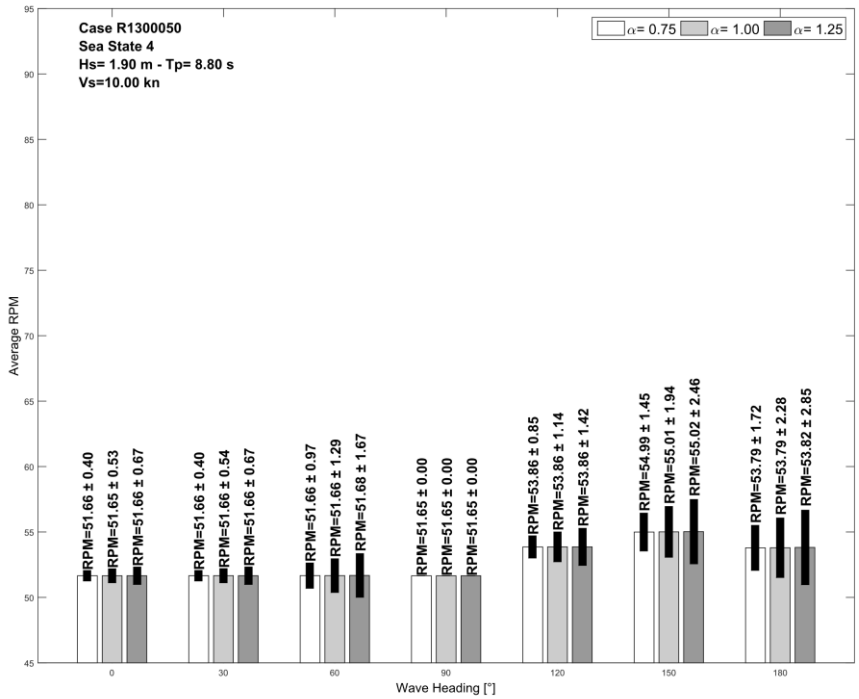

Figure 49: RPM variation for different α. Case 6 - Sea state 4 - Vessel speed 10kn.

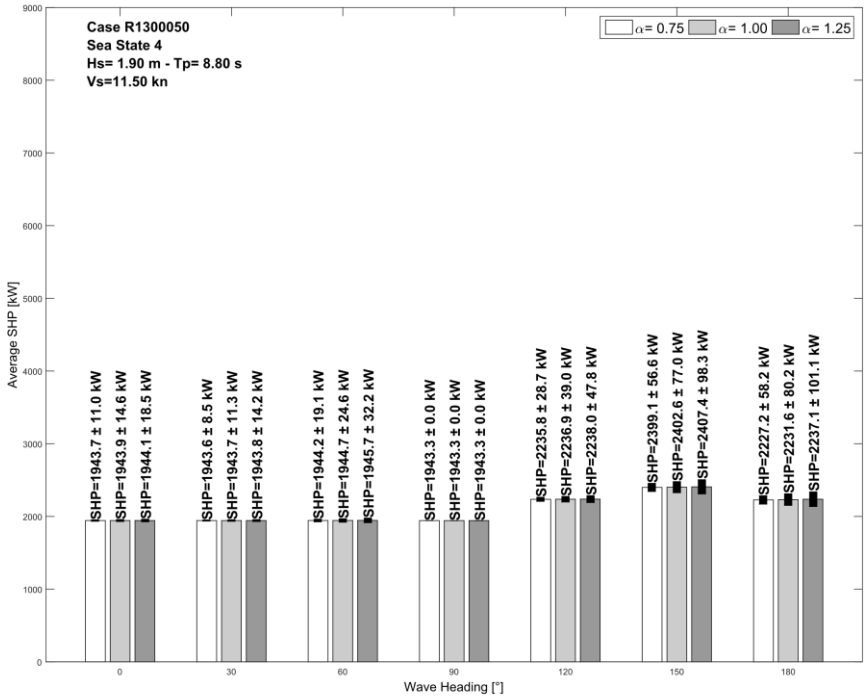

Figure 50: SHP variation for different α. Case 6 - Sea state 4 - Vessel speed 11.5kn.

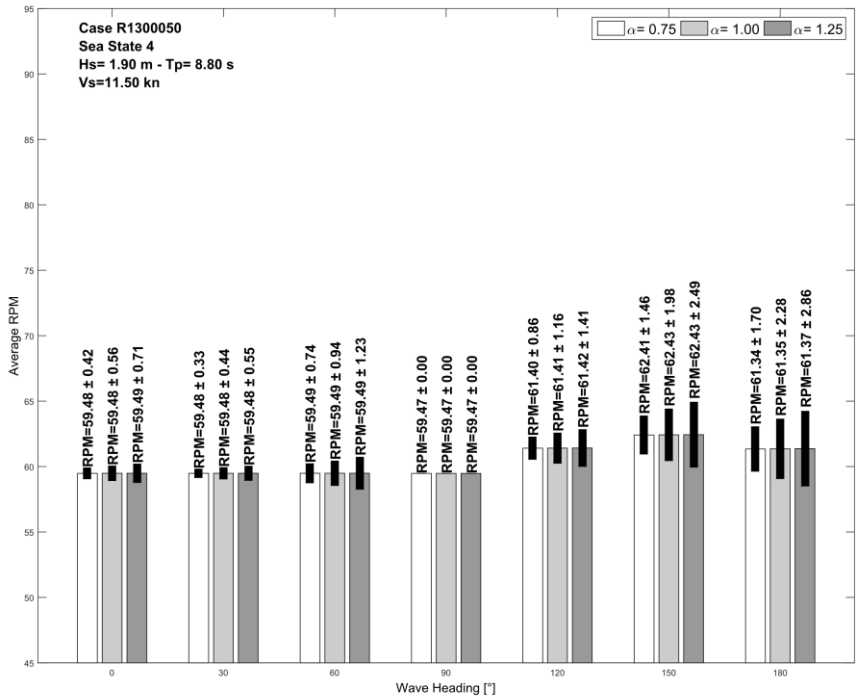

Figure 51: RPM variation for different α. Case 6 - Sea state 4 - Vessel speed 11.5kn.

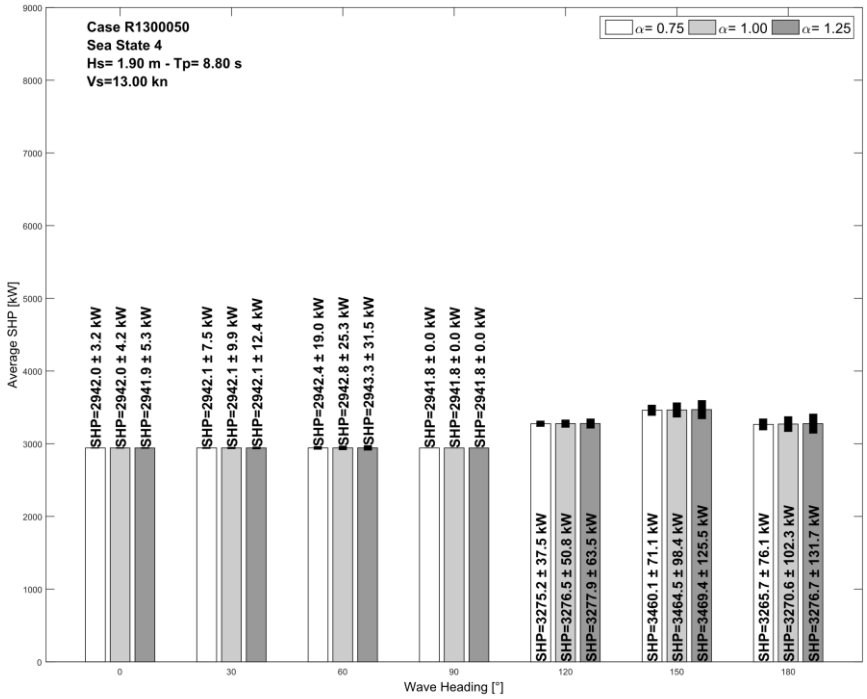

Figure 52: SHP variation for different α. Case 6 - Sea state 4 - Vessel speed 13kn.

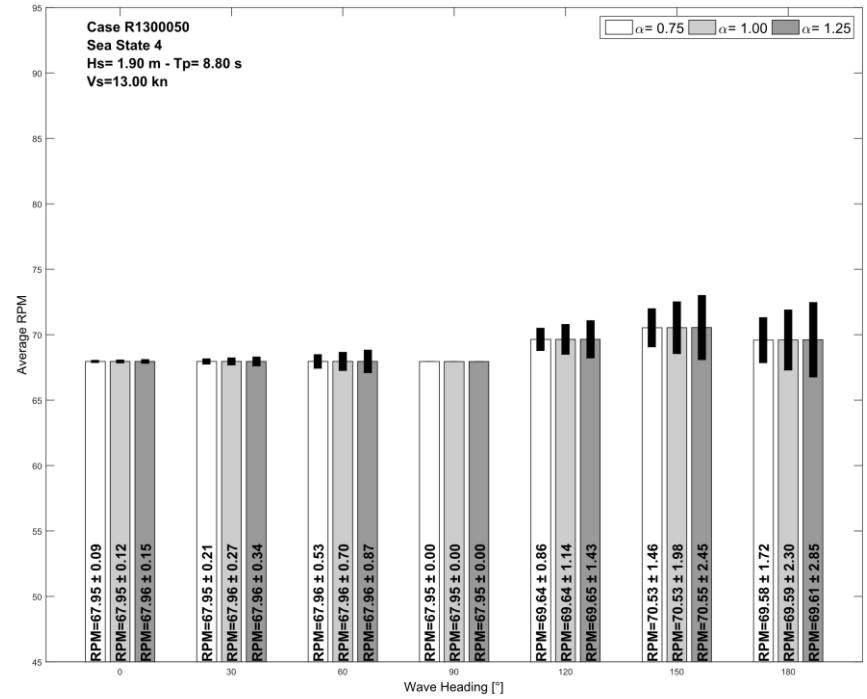

Figure 53: RPM variation for different α. Case 6 - Sea state 4 - Vessel speed 13kn.

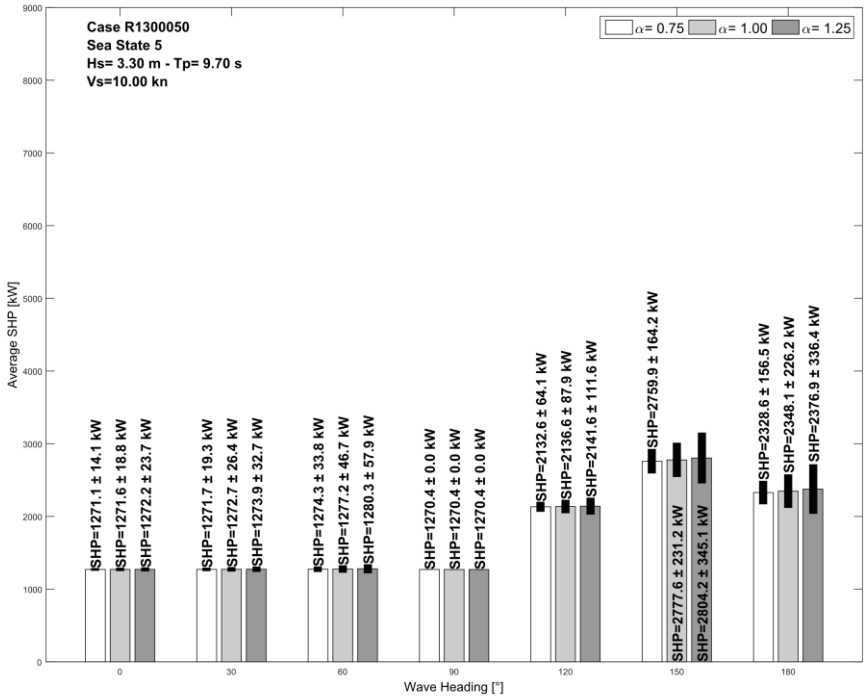

Figure 54: SHP variation for different α. Case 6 - Sea state 5 - Vessel speed 10kn.

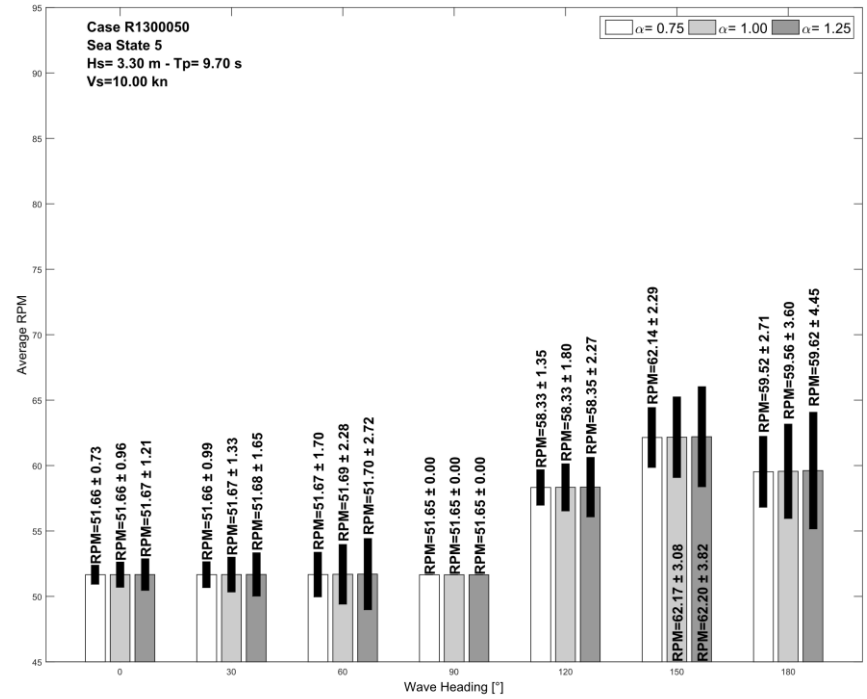

Figure 55: RPM variation for different α. Case 6 - Sea state 5 - Vessel speed 10kn.

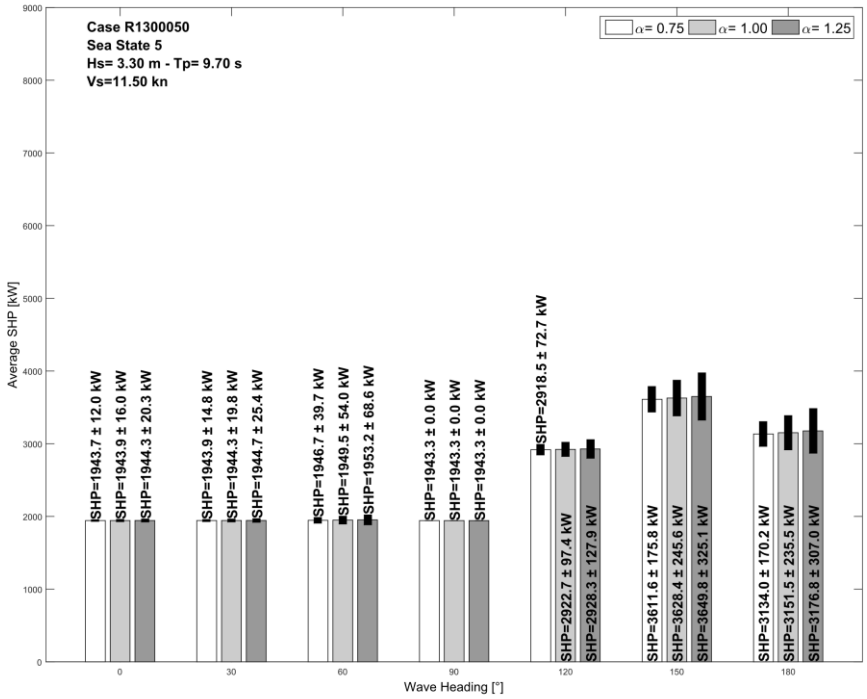

Figure 56: SHP variation for different α. Case 6 - Sea state 5 - Vessel speed 11.5kn.

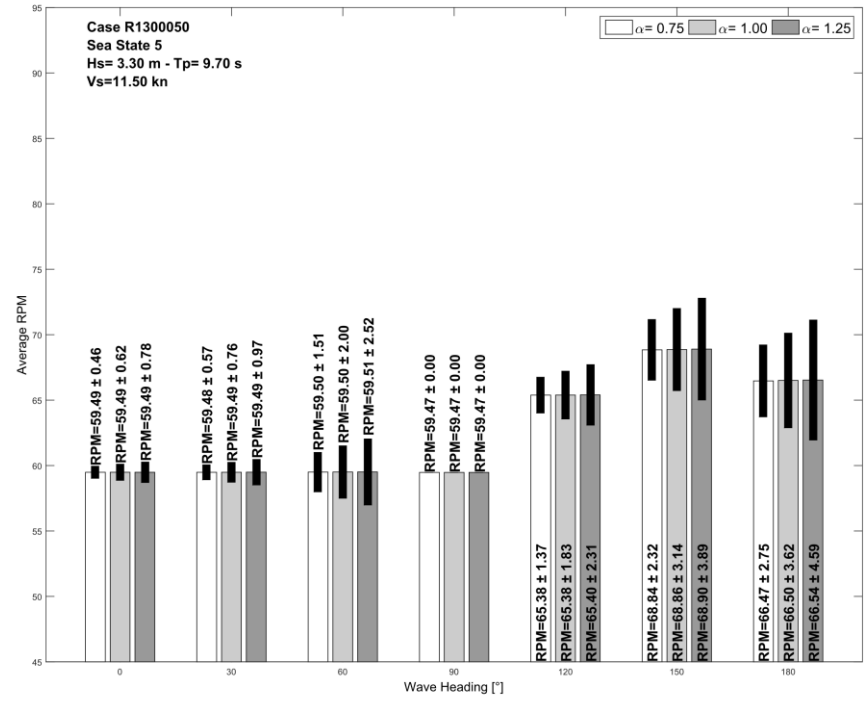

Figure 57: RPM variation for different α. Case 6 - Sea state 5 - Vessel speed 11.5kn.

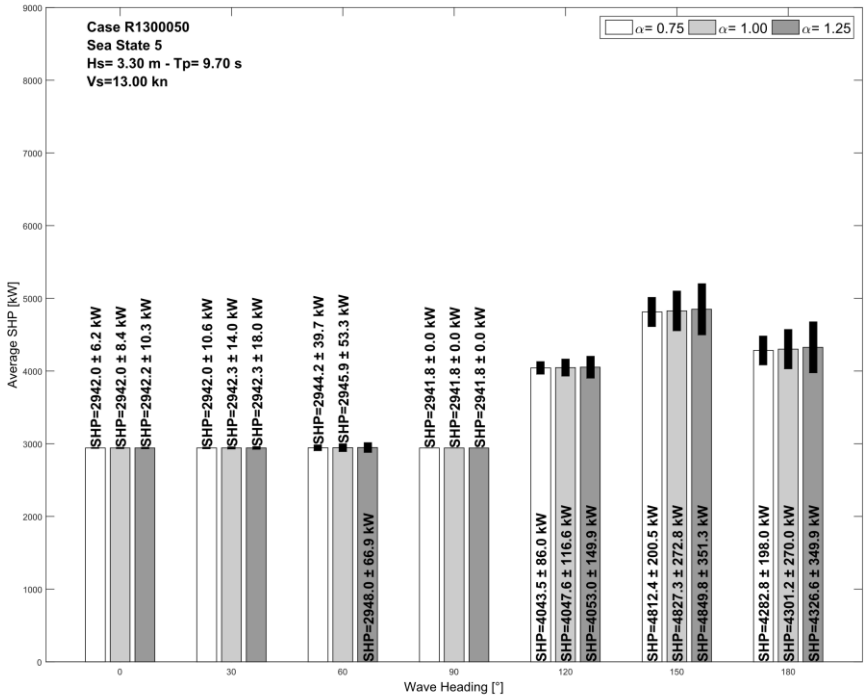

Figure 58: SHP variation for different α. Case 6 - Sea state 5 - Vessel speed 13kn.

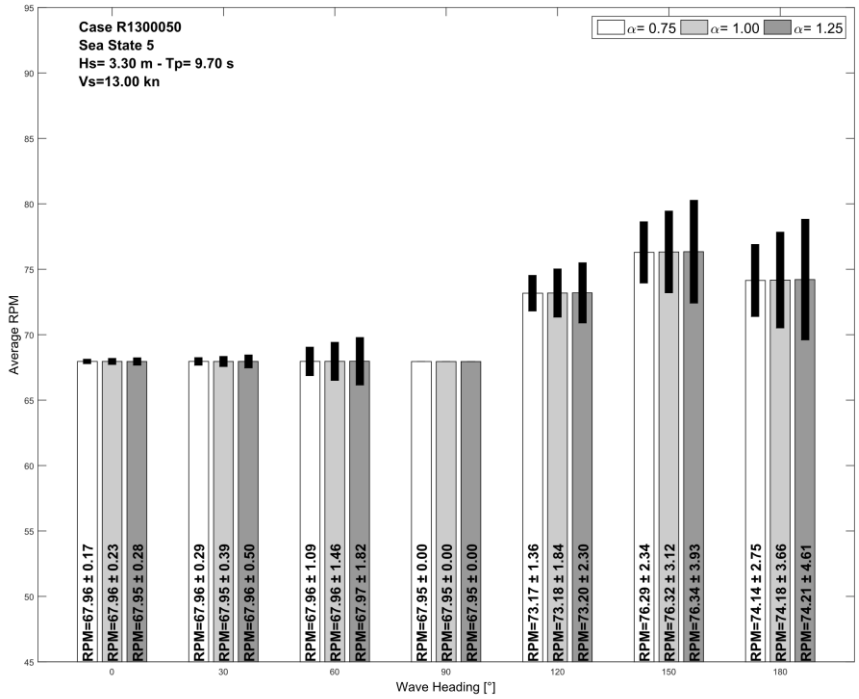

Figure 59: RPM variation for different α. Case 6 - Sea state 5 - Vessel speed 13kn.